# Eddy covariance data reveal that a small freshwater reservoir emits a substantial amount of carbon dioxide and methane

Alexandria G Hounshell[1,1], Brenda M D'Acunha[2,2], Adrienne Breef-Pilz[1,1], Mark S. Johnson[2,2], R. Quinn Thomas[1,1], and Cayelan Carey[1,1]

[1]Virginia Tech
[2]University of British Columbia

November 30, 2022

**Abstract**

Small freshwater reservoirs are ubiquitous and likely play an important role in global greenhouse gas (GHG) budgets relative to their limited water surface area. However, constraining annual GHG fluxes in small freshwater reservoirs is challenging given their footprint area and spatially and temporally variable emissions. To quantify the GHG budget of a small (0.1 km2) reservoir, we deployed an eddy covariance system in a small reservoir located in southwestern Virginia, USA over two years to measure carbon dioxide (CO2) and methane (CH4) fluxes near-continuously. Fluxes were coupled with in situ sensors measuring multiple environmental parameters. Over both years, we found the reservoir to be a large source of CO2 (633-731 g CO2-C m-2 yr-1) and CH4 (1.02-1.29 g CH4-C m-2 yr-1) to the atmosphere, with substantial sub-daily, daily, weekly, and seasonal timescales of variability. For example, fluxes were substantially greater during the summer thermally-stratified season as compared to the winter. In addition, we observed significantly greater GHG fluxes during winter intermittent ice-on conditions as compared to continuous ice-on conditions, suggesting GHG emissions from lakes and reservoirs may increase with predicted decreases in winter ice-cover. Finally, we identified several key environmental variables that may be driving reservoir GHG fluxes at multiple timescales, including, surface water temperature and thermocline depth followed by fluorescent dissolved organic matter. Overall, our novel year-round eddy covariance data from a small reservoir indicate that these freshwater ecosystems likely contribute a substantial amount of CO2 and CH4 to global GHG budgets.

# Eddy covariance data reveal that a small freshwater reservoir emits a substantial amount of carbon dioxide and methane

**Alexandria G. Hounshell[1, †], Brenda M. D'Acunha[2], Adrienne Breef-Pilz[1], Mark S. Johnson[2,3], R. Quinn Thomas[1,4], Cayelan C. Carey[1]**

[1] Department of Biological Sciences, Virginia Tech, Blacksburg, VA, USA, [2] Department of Earth, Ocean, and Atmospheric Sciences, University of British Columbia, Vancouver, BC, Canada, [3] Institute for Resources, Environment and Sustainability, University of British Columbia, Vancouver, BC, Canada, [4] Department of Forest Resources and Environmental Conservation, Virginia Tech, Blacksburg, VA, USA

Corresponding author: Alexandria G. Hounshell (alexgh@vt.edu)

† Current affiliation: National Centers for Coastal Ocean Science, National Oceanographic and Atmospheric Administration, Beaufort, NC, 28516 alexandria.hounshell@noaa.gov

**Key Points:**

- We measured high annual $CO_2$ (633-731g C $m^{-2}$ $yr^{-1}$) and $CH_4$ (1.02-1.29 g C $m^{-2}$ $yr^{-1}$) fluxes over 2 years from a small reservoir
- Fluxes were higher in the summer than winter, with statistically higher fluxes during intermittent ice-on as compared to continuous ice-on
- Surface water temperature, thermocline depth, and dissolved organic matter concentrations were correlated with reservoir fluxes

## Abstract

Small freshwater reservoirs are ubiquitous and likely play an important role in global greenhouse gas (GHG) budgets relative to their limited water surface area. However, constraining annual GHG fluxes in small freshwater reservoirs is challenging given their footprint area and spatially and temporally variable emissions. To quantify the GHG budget of a small (0.1 $km^2$) reservoir, we deployed an eddy covariance system in a small reservoir located in southwestern Virginia, USA over two years to measure carbon dioxide ($CO_2$) and methane ($CH_4$) fluxes near-continuously. Fluxes were coupled with *in situ* sensors measuring multiple environmental parameters. Over both years, we found the reservoir to be a large source of $CO_2$ (633-731 g $CO_2$-C $m^{-2}$ $yr^{-1}$) and $CH_4$ (1.02-1.29 g $CH_4$-C $m^{-2}$ $yr^{-1}$) to the atmosphere, with substantial sub-daily, daily, weekly, and seasonal timescales of variability. For example, fluxes were substantially greater during the summer thermally-stratified season as compared to the winter. In addition, we observed significantly greater GHG fluxes during winter intermittent ice-on conditions as compared to continuous ice-on conditions, suggesting GHG emissions from lakes and reservoirs may increase with predicted decreases in winter ice-cover. Finally, we identified several key environmental variables that may be driving reservoir GHG fluxes at multiple timescales, including, surface water temperature and thermocline depth followed by fluorescent dissolved organic matter. Overall, our novel year-round eddy covariance data from a small reservoir indicate that these freshwater ecosystems likely contribute a substantial amount of $CO_2$ and $CH_4$ to global GHG budgets.



## Plain Language Summary

Freshwater ecosystems release substantial amounts of greenhouse gases, especially carbon dioxide and methane, to the atmosphere. Small waterbodies, such as lakes and reservoirs, are common in the landscape and may release particularly high levels of greenhouse gases, though their overall contribution remains unknown. The most common methods to date for estimating greenhouse gas emissions from freshwaters typically involve only measuring concentrations during the daytime on a handful of days throughout the year. Thus, there is a clear need for near-continuous measurements of carbon dioxide and methane from small waterbodies throughout the year on multiple timescales (hours to years). To do this, we measured near-continuous fluxes of

carbon dioxide and methane from a small reservoir using eddy covariance over two years. We found this small reservoir to be a large source of both carbon dioxide and methane to the atmosphere over two years and found high variability in fluxes measured at short (sub-daily) to long (seasonal) timescales. Overall, this study demonstrates the importance of small reservoirs as greenhouse gas sources to the atmosphere and emphasizes the need for additional measurements to estimate their contribution to global greenhouse gas budgets.

## 1 Introduction

Freshwater ecosystems play a disproportionately large role in global greenhouse gas (GHG) budgets relative to their total water surface area, often emitting more GHGs than are taken up by terrestrial ecosystems (Bastviken et al. 2011; Cole et al. 2007; DelSontro et al. 2018; Tranvik et al. 2009). Despite their importance, however, the contribution of inland waters remains under-represented within global carbon (C) and GHG budgets (Butman et al. 2018; Deemer and Holgerson, 2021; Deemer et al. 2016; DelSontro et al. 2018). To date, most studies measuring GHG emissions from freshwater lakes and reservoirs are based on snapshot measurements from short-term floating chamber deployments or grab samples of dissolved GHGs, which are extrapolated to broad spatial and temporal scales to estimate annual whole-ecosystem fluxes (Bastviken et al. 2015; Klaus et al. 2019; Wik et al. 2016). While these approaches have provided useful insights into general patterns of GHG cycling in freshwater ecosystems, they are inherently limited in capturing the high spatial and temporal variability in freshwater GHG fluxes (A.K. Baldocchi et al. 2020; Butman et al. 2018; Klaus et al. 2019; Rosentreter et al. 2021; Wik et al. 2016).

Among freshwater ecosystems, small (<1 $km^2$) reservoirs may be particularly under-represented in GHG budgets (Deemer and Holgerson, 2021; DelSontro et al. 2018; Rosentreter al. 2021). It is estimated that there are ~5.8 million lakes and reservoirs in the contiguous U.S. (Winslow et al. 2014), of which approximately half (~2.6 million) are human-made reservoirs (Smith et al. 2002). Small reservoirs (<1 $km^2$) compose >71% of reservoirs in the United States (National Inventory of Dams, USACE 2021), indicating that these ecosystems are extremely common, with at least ~1.8 million small reservoirs in the conterminous U.S. However,

constraining annual GHG estimates in small freshwater reservoirs is challenging given their small footprint area and heterogeneous GHG emissions (Loken et al. 2019; McClure et al. 2020; Podgrajsek et al. 2015). Short-term measurements indicate the potential for these ecosystems to exhibit high, but patchy fluxes (Deemer and Holgerson, 2021; DelSontro et al. 2018; McClure et al. 2018, 2020; Rosentreter et al. 2021), but to the best of our knowledge their annual emissions remain largely unknown.

Eddy covariance (EC) systems are increasingly being deployed on lakes and reservoirs to constrain sub-daily GHG fluxes over large spatial footprints, enabling the quantification of whole-ecosystem GHG fluxes at multiple temporal scales (e.g., A.K. Baldocchi et al. 2020; Golub et al. 2021; Eugster et al. 2011; Vesala et al. 2011; Waldo et al. 2021). EC systems are used to determine the net exchange of carbon dioxide ($CO_2$), methane ($CH_4$), and/or other gases at sub-hourly time scales via micrometeorology and *in situ* atmospheric trace gas concentrations measured using infrared gas analyzers (A.K. Baldocchi et al. 2020; Golub et al. 2021; Vesala et al. 2011). By collecting near-continuous, high frequency data (typically measured at 10-20 Hz and reported as 30-minute means), EC systems allow GHG fluxes to be estimated at sub-daily to annual timescales, improving our understanding of GHG flux temporal variability beyond traditional discrete measurements (Golub et al. 2021; Reed et al. 2018; Vesala et al. 2011). Additionally, EC systems often capture a larger spatial footprint compared to traditional discrete measurements, as measured fluxes represent the average flux from the atmospherically-mixed area upwind of the deployed EC system (Golub et al. 2021, Waldo et al. 2021). Thus, EC systems can greatly increase the temporal and spatial resolution of measured fluxes in lakes and reservoirs, with the caveat that important considerations and data filtering are needed for EC systems in small waterbodies (Scholz et al. 2021). Specifically, a waterbody's small surface area increases the likelihood of surrounding terrestrial vegetation impacting EC measurements of aquatic fluxes and decreases the area available for a well-mixed, turbulent footprint (Esters et al. 2020; Scholz et al. 2021; Vesala et al. 2011).

While the majority of reported freshwater EC studies have been conducted on short timescales (days to months; e.g., Erkkilia et al. 2018; Gorsky et al. 2021; Jammet et al. 2015; Podgrajsek et al. 2014, 2015; Vesala et al. 2006, 2011), longer-term studies measuring $CO_2$ or $CH_4$ fluxes in lakes and reservoirs on annual timescales are now becoming more common (e.g., A.K. Baldocchi et al. 2020; Golub et al. 2021; Jammet et al. 2017; Liu et al. 2016; Reed et al.

2018; Shao et al. 2015; Scholz et al. 2021; Taoka et al. 2020; Waldo et al. 2021). An annual study conducted in Lake Erie, USA found this highly-eutrophic system was a small sink of $CO_2$ during the summer productive season yet ultimately a $CO_2$ source on annual timescales (Shao et al. 2015). Other studies have highlighted the importance of short (hourly to daily), episodic events on annual $CO_2$ budgets, including the disproportionate effect of storms on annual $CO_2$ emissions from a large subtropical reservoir (Liu et al. 2016), fall mixing in a large (40 $km^2$) temperate lake (Reed et al. 2018), and pulses of $CH_4$ following ice-off in a north temperate lake (Gorsky et al. 2021). Annual studies have also revealed low and relatively consistent $CO_2$ fluxes during the winter ice-covered period (A.K. Baldocchi et al. 2020; Reed et al. 2018). In addition to noted diel, seasonal, and episodic variability in $CO_2$ fluxes, two annual studies recently found the sub-monthly timescale to be an important timescale of variability, though the mechanism for this variability remains unknown (A.K. Baldocchi et al. 2020; Golub et al. 2021). Despite the increase in studies using EC systems to measure $CO_2$ and $CH_4$ fluxes from freshwaters, few studies to date have captured both $CO_2$ and $CH_4$ fluxes on the annual scale, especially during winter.

Measuring annual-scale $CO_2$ and $CH_4$ fluxes is particularly important as GHG fluxes are likely rapidly changing due to altered climate (Bartosiewicz et al. 2019; Beaulieu et al. 2019), motivating several potential hypotheses for how different environmental drivers may alter fluxes. Multiple drivers sensitive to climate change likely affect GHG fluxes, though annual-scale studies to test the effects of these drivers on fluxes across multiple timescales are lacking. For example, increasing surface temperatures and changes in precipitation and nutrient loading are changing phytoplankton productivity and allochthonous C inputs to lakes and reservoirs (Fowler et al. 2020; Hanson et al. 2015; Tranvik et al. 2009). Changes in freshwater primary production and nutrient inputs to freshwater systems have been directly linked to changes in $CO_2$ (DelSontro et al. 2018), as well as $CH_4$ emissions (Deemer and Holgerson, 2021; DelSontro et al. 2018; McClure et al. 2020). Finally, increasing air temperatures are leading to warmer winters and more intermittent and partial ice cover (Imrit and Sharma, 2021; Sharma et al. 2021; Woolway et al. 2020), highlighting the need to understand the role of ice in constraining GHG fluxes. All these examples emphasize the importance of measuring near-continuous GHG fluxes on the annual scale along with key potential environmental drivers, such as precipitation and freshwater inflows, air and water temperature, chlorophyll-*a*, dissolved organic matter, and ice-on/ice-off as

potential GHG drivers, as it is likely that some drivers may have a greater effect at certain timescales than others.

Altogether, there is a clear need to measure annual-scale $CH_4$ and $CO_2$ fluxes from small freshwater ecosystems, especially small reservoirs. To the best of our knowledge, only one freshwater study has measured both $CH_4$ and $CO_2$ fluxes on an annual timescale (Jammet et al. 2017), while Waldo et al. (2021) measured only $CH_4$ fluxes at the annual scale. Waldo et al. (2021) used EC to measure annual $CH_4$ fluxes from a large (2.4 $km^2$), highly-eutrophic temperate reservoir, measuring emissions up to 71.4 g $CH_4$ $m^{-2}$ $yr^{-1}$, which is in the top quarter of those reported from lakes and reservoirs to date. In an Arctic lake, Jammet et al. (2017) used EC to measure low GHG fluxes during ice cover, followed by large $CH_4$ and $CO_2$ fluxes during spring-thaw, and increasing ebullitive $CH_4$ fluxes during the ice-free season concurrent with high rates of $CO_2$ uptake due to photosynthesis. Aggregated across the full year, this Arctic lake was a net source of both $CH_4$ and $CO_2$ to the atmosphere (Jammet et al. 2017). Across the literature, most EC studies have focused on naturally-formed lakes, and all EC reservoir studies of which we are aware (Eugster et al. 2011; Golub et al. 2021; Liu et al., 2016; Waldo et al. 2021) were conducted in large (>2.4 $km^2$) reservoirs.

To better understand the GHG budgets of small reservoirs and identify key environmental drivers, we deployed an EC system in a small (0.1 $km^2$) freshwater reservoir located in southwestern Virginia, USA for two years to measure $CO_2$ and $CH_4$ fluxes near-continuously. Flux measurements were coupled with *in situ* sensors measuring multiple environmental parameters, including surface water temperature, dissolved oxygen, chlorophyll-*a*, and fluorescent dissolved organic matter. We used the measured GHG fluxes to answer the questions: 1) What is the annual phenology of $CO_2$ and $CH_4$ fluxes in a small, eutrophic reservoir, including during the critical winter period?; and 2) Which environmental variables best explain $CO_2$ and $CH_4$ variability at daily to monthly timescales?

## 2 Materials and Methods

### 2.1 Site description

Falling Creek Reservoir (FCR) is a small, eutrophic reservoir located in Vinton, Virginia, USA (Fig. 1; 37.30ºN, 79.84ºW; Howard et al. 2021). The reservoir and surrounding forested watershed are owned and operated by the Western Virginia Water Authority (WVWA) as a primary drinking water source (Gerling et al. 2016). FCR has a surface area of 0.119 $km^2$ and maximum depth of 9.3 m (McClure et al. 2018). The reservoir is dimictic and thermally stratified from April to October (McClure et al. 2018). During the study period, water was not extracted for drinking water treatment and remained at a constant full-pond level.

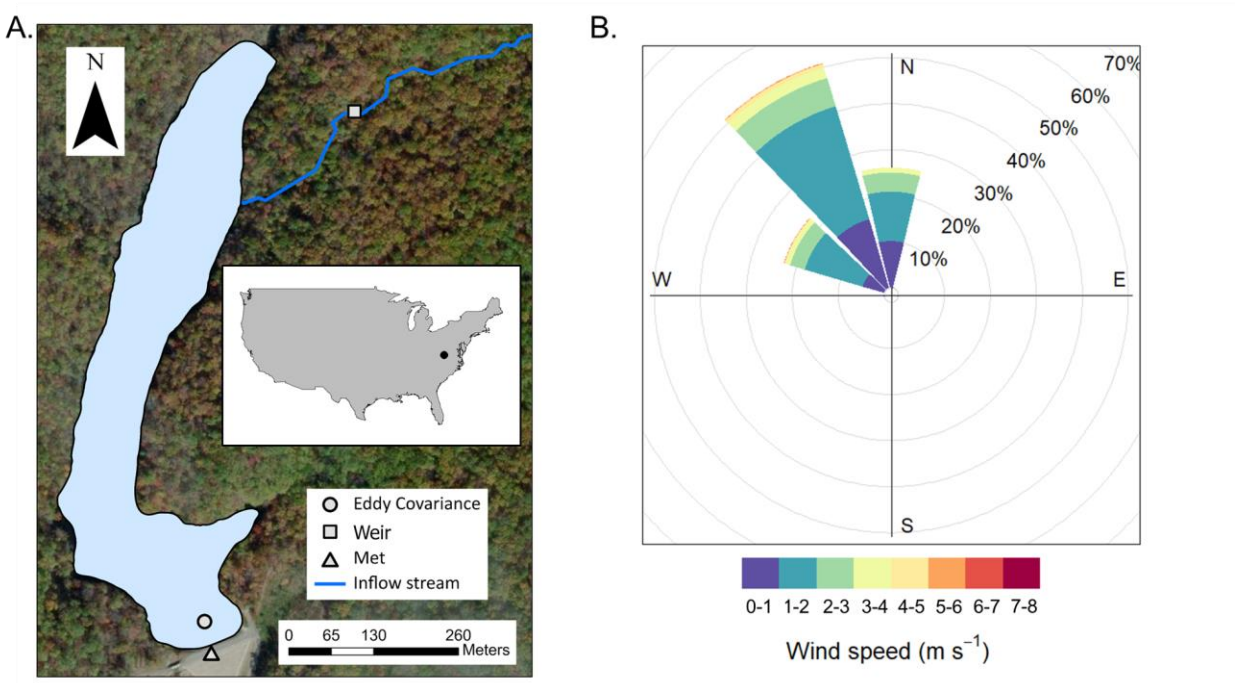


**Figure 1.** A. Map of Falling Creek Reservoir (FCR) located in Vinton, Virginia, USA (map inset) showing location of the eddy covariance system, the weir located on the primary freshwater inflow, and the meteorological station located on the dam. B. Wind rose showing the dominant wind direction and wind speed (m $s^{-1}$) of greenhouse gas fluxes retained for analysis. The cumulative footprint distribution for the whole study period is shown in the supplementary information (Fig. S1).

## 2.2 Data collection and overview

We used an EC system to measure $CO_2$ and $CH_4$ fluxes between the water surface and the atmosphere from 1 May 2020 to 30 April 2022 (details below; Carey et al. 2022a). To complement the EC measured fluxes, we also calculated $CO_2$ and $CH_4$ diffusive gas fluxes using dissolved $CO_2$ and $CH_4$ discrete grab samples collected during daylight hours (between ~0800 to 1300) weekly to monthly from the water's surface at the deepest site of the reservoir, located near the dam, throughout the 2-year study period (details below; Carey et al. 2022b).

In addition to the EC and diffusive fluxes, we also collected meteorological and environmental data. Briefly, a Campbell Scientific (Logan, Utah, USA) research-grade meteorological station measured air temperature; relative humidity; air pressure; wind speed and direction; upwelling and downwelling shortwave and longwave radiation; total rainfall; photosynthetically-active radiation (PAR); and albedo every minute at the reservoir dam (sensor information provided by Carey et al. 2022c). At the reservoir's deepest site, we collected 10-minute water temperature measurements every 1 m from the surface (0.1 m) to just above the sediments (9 m) using a thermistor string. Thermistor data were used to calculate the difference in temperature between 0.1 m and 9.0 m (Diff. Temp) and daily buoyancy frequency ($N^2$), two metrics of thermal stratification, as well as thermocline depth throughout the study period (May 2020 to April 2022) using the LakeAnalyzer package in R (Winslow et al. 2016a). Fall turnover was defined as the first day in autumn when the temperature at 1 m was $<1^oC$ of the temperature measured at 8 m (1 November 2020 and 3 November 2021; McClure et al. 2018). Spring mixing was harder to identify due to intermittent ice-on in 2021, but we defined spring mixing as the first day in spring after complete ice-off when the temperature at 1 m was $<1^oC$ of the temperature measured at 8 m (26 February 2021 and 10 February 2022). Ice cover was determined by the presence of inverse stratification coupled with higher albedo and verified by visual observation, described by Carey and Breef-Pilz (2022).

Water column temperature data complemented 10-minute measurements of dissolved oxygen (DO) percent saturation, chlorophyll-*a* (Chl-*a*, µg $L^{-1}$), and fluorescent dissolved organic matter (fDOM, relative fluorescent units, RFU) measured using an EXO2 sonde (YSI, Yellow Springs, Ohio, USA) deployed at 1.6 m (Carey et al. 2022d). The EXO2 sonde was removed

from the reservoir on 2 December 2020 for annual sensor maintenance and re-deployed on 27 December 2020. Finally, we measured stream inflow every 15 minutes on the primary inflowing stream to the reservoir via a gaged v-notch weir fitted with a Campbell Scientific CS451 pressure transducer (Campbell Scientific, Logan, Utah, USA), which was used to calculate the 15-minute flow rate following (Carey et al. 2022e). The weir was breached on 20 July 2020 and repaired on 24 August 2020, resulting in no flow data during this interval.

### 2.3 Eddy covariance flux measurements

An EC system was deployed above the water surface over the deepest portion of the reservoir from 1 May 2020 to 30 April 2022. The EC instrumentation was installed on a permanent metal platform that extends ~45 m from the dam and 2.9 m over the reservoir's surface. As noted above, the reservoir was maintained at full pond, resulting in a consistent height of the EC system over the water's surface during the study period. The EC system included an ultrasonic anemometer to measure 3D wind speed and direction (CSAT3, Campbell Scientific), an open-path infrared gas analyzer for measuring $CH_4$ concentration (LI-7700, LiCor Biosciences, Lincoln, Nebraska, USA), and an enclosed-path infrared gas analyzer for measuring $CO_2$ and water vapor concentrations (LI-7200, LiCor Biosciences), all recorded at 10 Hz by a data logger (LI-7550, LiCor Biosciences). On 10 August 2020, the data logger was removed for maintenance and re-deployed on 2 September 2020. Additionally, a thermocouple on the $CO_2$ sensor (LI-7200) was inoperable starting on 5 April 2021 and was repaired on 26 April 2021.

The raw 10-Hz data were first processed into 30-minute fluxes using the EddyPro v.7.0.6 software (LiCor Biosciences 2019). Fluxes were calculated following standard methods in EddyPro v.7.0.6 (LiCor Biosciences 2019), which included spike detection and removal (Vickers and Mahrt, 1997), a double rotation for tilt correction (Wilczak et al. 2001), linear detrending (Gash and Culf, 1996), time lag compensation, and spectral corrections for high and low-pass filtering effects following Moncrieff et al. (2004) and Moncrieff et al. (1997), respectively. In addition, $CH_4$ molar density was corrected to account for air density fluctuations and spectroscopic effects of temperature, pressure and water vapor following Webb et al. (1980).

This correction was not needed for $CO_2$, as fluxes were estimated using mixing ratios instead of densities (Burba et al. 2012).

Following initial flux calculations and processing in EddyPro, we conducted additional data processing following standard best practices, including: 1) removing wind directions which originated outside of the reservoir (80-250°; Fig. 1); 2) removing extreme flux values ($CO_2$ fluxes $\geq |100|$ μmol C $m^{-2}$ $s^{-1}$; $CH_4$ fluxes $\geq |0.25|$ μmol C $m^{-2}$ $s^{-1}$); 3) removing $CH_4$ fluxes when signal strength <20%; 4) removing $CO_2$ and $CH_4$ fluxes when they did not pass the test for stationarity or developed turbulent conditions (QC, quality control level 2 per Mauder and Foken, 2006), in addition to when the latent heat (LE) or sensible heat flux (H) had QC level <2; 5) removing open-path $CH_4$ fluxes during periods of rainfall, which was determined based on the rain gauge deployed at the dam; 6) removing additional periods of low turbulence friction velocity ($u_*$), as described below; and 7) removing data that corresponded to flux footprints that extended significantly beyond the reservoir.

Finally, we used REddyProc (Wutzler et al. 2021) to determine the $u_*$ threshold for sufficiently turbulent conditions and removed any fluxes where $u_*$ was < 0.075 m $s^{-1}$. To account for the uncertainty of estimating the $u_*$ threshold, we used bootstrapping to estimate the distribution of $u_*$ thresholds, and obtained the $5^{th}$, $50^{th}$ and $95^{th}$ percentiles of this distribution (0.070, 0.075, and 0.163 m $s^{-1}$, respectively; Wutzler et al., 2018).

Flux footprints were modeled for each half-hour using a simple, two-dimensional parameterization developed by Kljun et al. (2015) (Fig. S1). This model builds on the Lagrangian stochastic particle dispersion model (Kljun et al. 2002), and provides information on the extent, width, and shape of the footprint. All the variables needed for the model were obtained directly from the dataset described above or calculated following Kljun et al. (2015). Fluxes were excluded when the along-wind distance providing 90% cumulative contribution to turbulent fluxes was outside the reservoir, based on the footprint analysis. We chose to use this filtering threshold given the challenges of modeling footprints in small reservoirs; consequently, our fluxes are likely conservative. All post-processing analyses were conducted using R

statistical software (v.4.0.3). Code for post-processing and all EC data can be found in the Environmental Data Initiative (EDI) repository (Carey et al. 2022a).

### 2.4 Diffusive flux measurements

We estimated discrete diffusive fluxes from FCR using dissolved $CO_2$ and $CH_4$ samples (Carey et al. 2022b) collected at the surface of the reservoir to compare with EC fluxes. Surface water samples were collected at 0.1 m depth using a 4-L Van Dorn sampler (Wildlife Supply Co., Yulee, Florida, USA) adjacent to the EC sensors (Fig. 1). Replicate (n=2) water samples were collected via a Van Dorn sampler into 20-mL serum vials without headspace, immediately capped, and then stored on ice until analysis within 24 hours. Samples were analyzed following Carey et al. (2022b) on a Shimadzu Nexis GC-2030 Gas Chromatograph (Kyoto, Japan) with a Flame Ionization Detector (GC-FID) and Thermal Conductivity Detector (TCD).

The measured surface samples were used to calculate $CO_2$ and $CH_4$ diffusive fluxes from the surface of FCR into the atmosphere on each day of sample collection following the equation:

$$\text{Flux} = k * (C_{eq} - C_{air}) \quad \text{Eq. 1}$$

where k is the gas transfer velocity (m $d^{-1}$) corrected for temperature and gas species ($CO_2$ or $CH_4$, respectively), $C_{eq}$ is the concentration of $CO_2$ or $CH_4$ at the reservoir surface (0.1 m), and $C_{air}$ is the atmospheric concentration of $CO_2$ or $CH_4$ measured by the EC system (Cole and Caraco, 1998). The k value was calculated for each time point using multiple methods included in the LakeMetabolizer package in R (Cole and Caraco, 1998; Crusius and Wannikof 2003; Heiskanen et al. 2014; MacIntyre et al. 2010; Read et al. 2012; Soloviev et al. 2007; Vachon and Prairie, 2013; Winslow et al. 2016b, 2016c). Both surface GHG replicates (n=2) calculated with each k method, were used to calculate fluxes; the resultant mean and standard deviation are reported.

### 2.5 Statistical analyses

To assess the phenology of fluxes ($CO_2$ and $CH_4$), we analyzed the mean and standard deviation (±1 S.D.) of measured EC fluxes at half-hourly, daily, weekly, and monthly time scales through the study period. For both EC and discrete diffusive fluxes, negative fluxes correspond

to fluxes into the reservoir (i.e., uptake) while positive fluxes are out of the reservoir (i.e., release to the atmosphere).

To assess diel variation in GHG fluxes, we compared median measured EC fluxes during the day (1100 to 1300) and night (2300 to 0100) throughout the year. As data were not normally distributed, we used paired Wilcoxon signed-rank tests to assess statistical significance of paired day-night fluxes. Additionally, we compared dawn (0500 to 0700) and dusk (1700 to 1900) median EC measured fluxes using the same methods.

Ice coverage at FCR is episodic and ephemeral, encompassing longer ice-covered periods as well as shorter-duration ice-covered periods when ice may be present during portions of sequential days or with partial coverage of the reservoir's surface, which we refer to as intermittent ice-on periods. To explore the role of variable winter ice cover on $CO_2$ and $CH_4$ fluxes, we analyzed mean half-hourly fluxes (±1 S.D.) from 10 January to 10 February for both 2021 and 2022, which encompassed a period of intermittent (2021) and continuous (2022) ice-on (following Carey and Breef-Pilz 2022; Table S1). We used Mann-Whitney-Wilcoxon tests to determine statistically-significant differences ($\alpha = 0.05$) between the median half-hourly fluxes measured during intermittent and continuous ice-on periods.

Finally, we calculated the net annual flux balance for $CO_2$ and $CH_4$ using both measured and gap-filled half-hourly EC data. Fluxes were summed across each year (01 May - 30 April). The standard deviation (±1 S.D.) was calculated for the measured and gap-filled data using the different u* scenarios. Briefly, half-hourly fluxes were gap-filled in REddyProc using the marginal distribution sampling method (MDS), which uses the correlation of measured fluxes with environmental driver variables, namely, light, moisture, and temperature to estimate fluxes during the missing periods (Wutzler et al. 2018). Gap-filling was performed for each of the u* scenarios, providing information about the uncertainty that might be introduced to the data by choosing a u* threshold.

### 2.6 Time series analysis

To identify key environmental predictors and test mechanistic relationships between observed mean daily, weekly, and monthly measured $CO_2$ and $CH_4$ fluxes and environmental

variables, we developed separate autoregressive integrated moving average (ARIMA) models for each timescale. ARIMA models are used to identify key environmental predictors while accounting for temporal autocorrelation (Hyndman and Athanasopoulos, 2018). We selected several potential environmental predictors, including: surface water temperature (Temp, 0.1 m, $^{o}$C); the difference between surface (0.1 m) and bottom (9 m) water temperatures (Diff. Temp); buoyancy frequency ($N^2$); thermocline depth (TD); DO percent saturation (DO sat); Chl-*a*; fDOM; and discharge (Inflow) measured at the primary inflow to FCR (Fig. S2, S3). Prior to ARIMA modeling, we conducted pairwise Spearman correlations on all predictor variables (aggregated to each time scale) and removed collinear variables (Pearson's rho≥0.7) that were the least correlated with fluxes. $N^2$ and Diff. Temp were removed for all time scales due to their strong correlation with surface water temperature (Table S2). Response and predictor variables were checked for skewness, transformed if appropriate, and normalized (z-scores) prior to model fitting (Hounshell et al. 2022).

We used a model selection algorithm (Lofton et al. 2022) to identify the importance of environmental predictor variables at each time scale. The algorithm was based on the auto.arima function in the forecast package in R (Hyndman and Khandakar, 2008; Hyndman et al. 2021) which compared fitted models to a global model (all possible predictors) and a null persistence model with just one autoregressive term (AR(1)). We selected the environmental model with the lowest corrected Akaike information criterion (AICc), as well as models within 2 AICc units (Burnham and Anderson, 2002). Models were limited to include one autoregressive term (Hounshell et al. 2022).

## 3 Results

Overall, due to data processing and filtering described above, including the 90% footprint restriction, EC fluxes captured 23% and 19% of total $CO_2$ and $CH_4$ fluxes, respectively, over two years from FCR (Table S3), which is similar to previously-reported deployments of EC systems at lakes and reservoirs (e.g., Golub et al. 2021; Reed et al. 2018; Waldo et al. 2021). The percentage of available data was relatively consistent across the daily timescale (from 0000 to 2330), ranging from 14%-34% of data availability for $CO_2$ (2200 and 1230, respectively) and

11%-32% for $CH_4$ (2200 and 1230, respectively; Fig. S4). We note that during the day, the dominant wind direction was outside the reservoir footprint, while the dominant wind direction was largely along the reservoir at night (Fig. S5). This pattern resulted in a high percentage of daytime fluxes removed due to wind direction, but overall, we observed a roughly equal contribution of day and night fluxes following all flux removal processes (i.e., flux filtering due to low u*). Data availability after filtering was also relatively consistent throughout seasons and between years, ensuring even representation of measured fluxes throughout the year (Fig. S6). We do note low data availability (<10%) for both $CO_2$ and $CH_4$ during August 2020, due to instrument maintenance, and for $CH_4$ during December 2020 and February 2021.

### 3.1 Phenology of $CO_2$ and $CH_4$ fluxes

High-frequency EC data show that FCR was generally a net source of both $CO_2$ and $CH_4$ to the atmosphere throughout the study period (Figs. 2, 3, S7; Tables S4). Overall, measured $CO_2$ fluxes ranged from -39.46 to 52.67 μmol $m^{-2}$ $s^{-1}$ with a mean flux of 1.86 ± 6.21 μmol $m^{-2}$ $s^{-1}$ (±1 S.D.) aggregated over the entire 2-year study period. Measured $CH_4$ fluxes ranged from -0.084 to 0.096 μmol $m^{-2}$ $s^{-1}$, with a mean $CH_4$ flux of 0.003 ± 0.011 μmol $m^{-2}$ $s^{-1}$ over the study period (Fig. 2, 3, S7; Table S4).

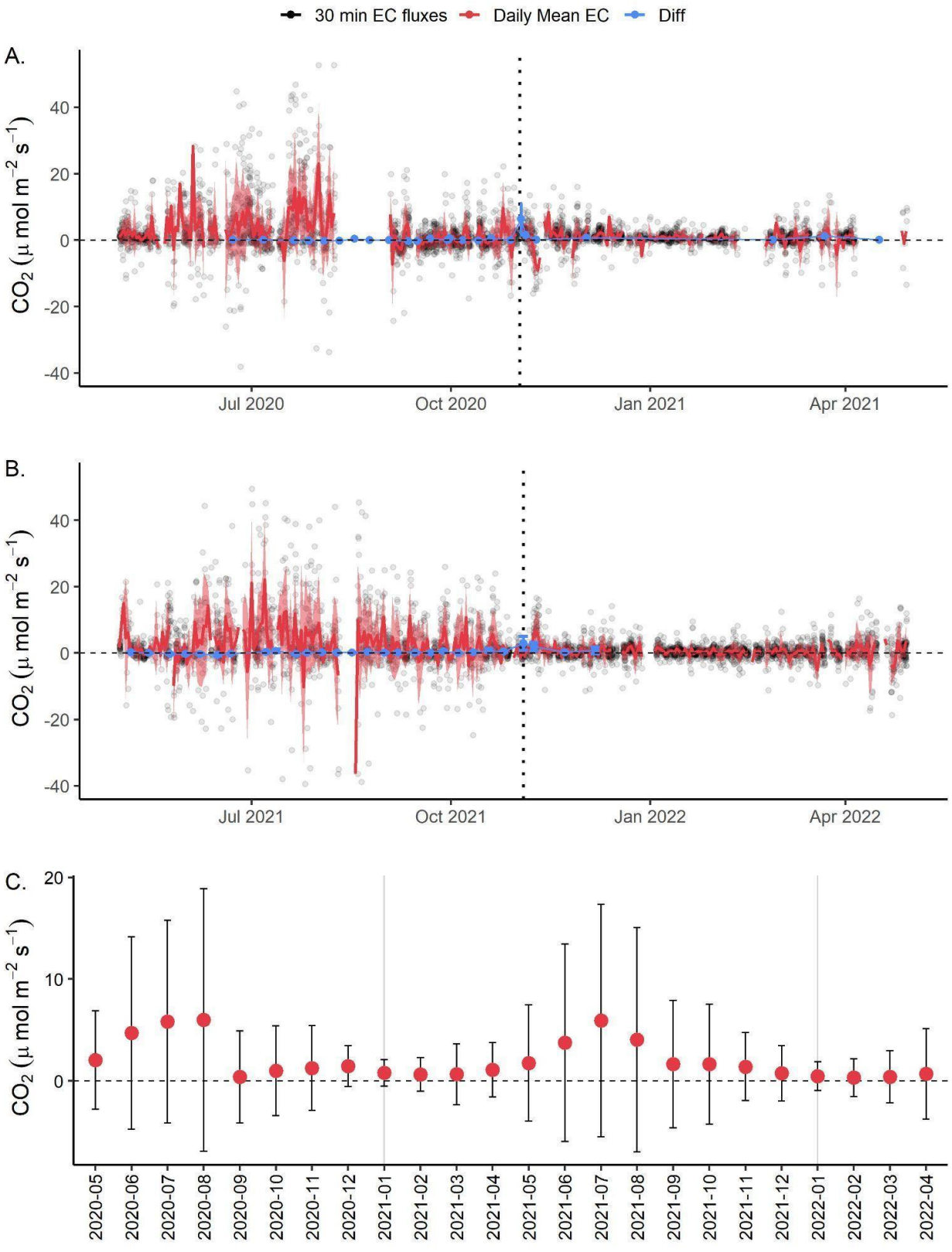
30 min EC fluxes
Daily Mean EC
Diff
A.
B.
C.
$CO_2$ (μ mol $m^{-2}$ $s^{-1}$)
40
20
0
-20
-40
Jul 2020
Oct 2020
Jan 2021
Apr 2021
Jul 2021
Oct 2021
Jan 2022
Apr 2022
10
2020-05
2020-06
2020-07
2020-08
2020-09
2020-10
2020-11
2020-12
2021-01
2021-02
2021-03
2021-04
2021-05
2021-06
2021-07
2021-08
2021-09
2021-10
2021-11
2021-12
2022-01
2022-02
2022-03
2022-04

365

**Figure 2.** Daily mean carbon dioxide fluxes ($CO_2$, μmol $m^{-2}$ $s^{-1}$) for A. May 2020 to April 2021 (Year 1) and B. May 2021 to April 2022 (Year 2) measured using eddy covariance (Daily Mean EC, red) and calculated discrete diffusive fluxes (Diff, blue) using the mean and standard deviation of seven gas transfer coefficient models (k; Winslow et al. 2016b). Grey dots represent measured half-hourly fluxes from the EC. The dark red line represents daily mean fluxes. The shaded red area represents ±1 standard deviation of the daily 30-minute fluxes using measured EC fluxes. The vertical dotted line indicates reservoir fall turnover. C. Mean monthly $CO_2$ fluxes (μmol $m^{-2}$ $s^{-1}$) aggregated from measured EC data. The error bars correspond to ±1 S.D. of aggregated fluxes for both measured and gap-filled EC values. The horizontal dashed line indicates zero fluxes.

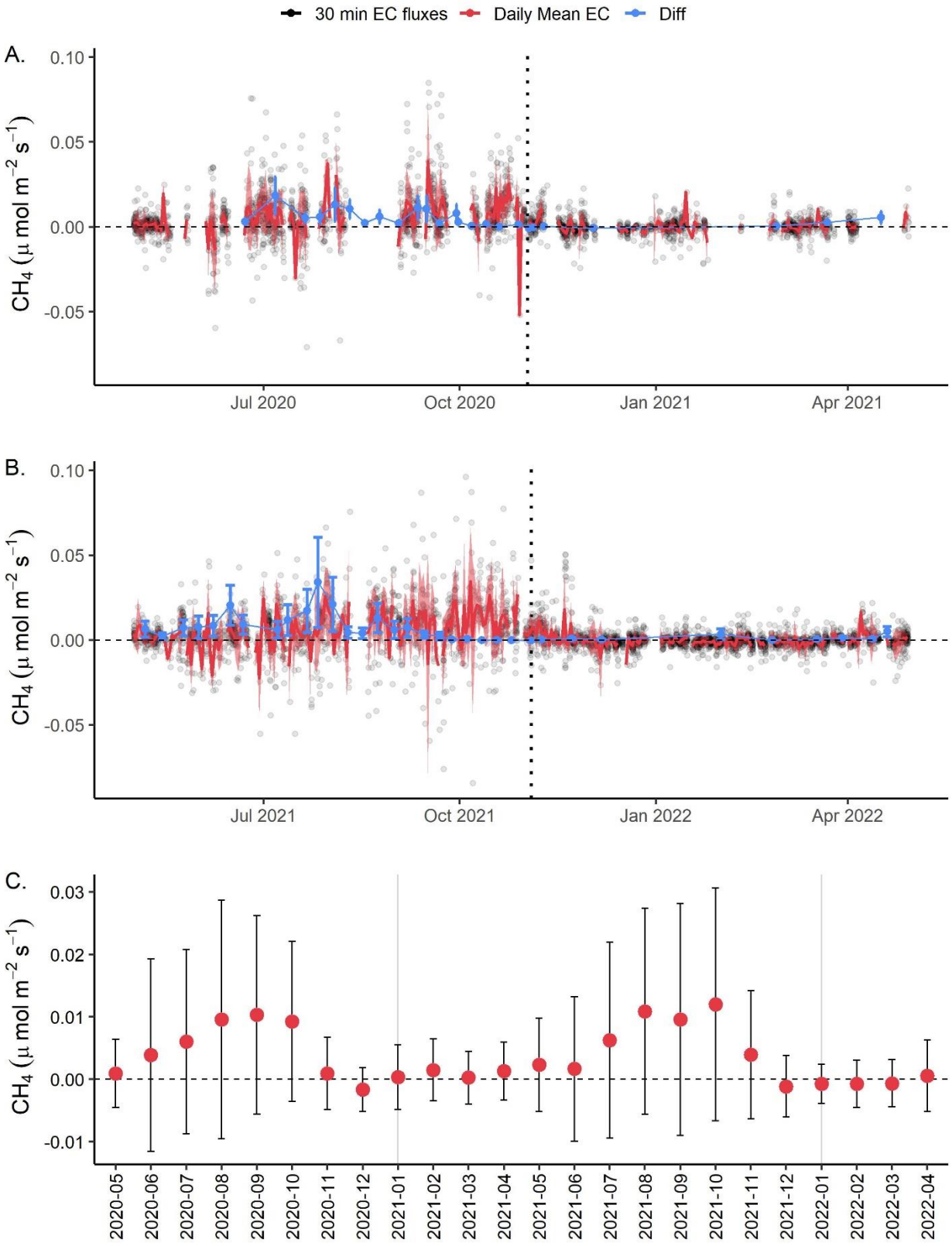
30 min EC fluxes
Daily Mean EC
Diff
A.
B.
C.
$CH_4$ ($\mu$ mol $m^{-2}$ $s^{-1}$)
0.10
0.05
0.00
-0.05
Jul 2020
Oct 2020
Jan 2021
Apr 2021
Jul 2021
Oct 2021
Jan 2022
Apr 2022
0.03
0.02
0.01
-0.01
2020-05
2020-06
2020-07
2020-08
2020-09
2020-10
2020-11
2020-12
2021-01
2021-02
2021-03
2021-04
2021-05
2021-06
2021-07
2021-08
2021-09
2021-10
2021-11
2021-12
2022-01
2022-02
2022-03
2022-04

376

**Figure 3.** Daily mean methane fluxes ($CH_4$, μmol $m^{-2}$ $s^{-1}$) for A. May 2020 to April 2021 (Year 1) and B. May 2021 to April 2022 (Year 2) measured using eddy covariance (Daily Mean EC, red) and calculated discrete diffusive fluxes (Diff, blue) using the mean and standard deviation of seven gas transfer coefficient models (k; Winslow et al. 2016b). Grey dots represent measured half-hourly fluxes from the EC. The dark red line represents daily mean fluxes. The shaded red area represents ±1 standard deviation of the daily 30-minute fluxes. The vertical dotted line indicates reservoir fall turnover for each year. C. Mean monthly $CH_4$ fluxes (μmol $m^{-2}$ $s^{-1}$) aggregated from measured EC data. The error bars correspond to ±1 S.D. of aggregated fluxes for both measured and gap-filled EC values. The horizontal dashed line indicates zero fluxes.

At the hourly to diel scale, we found that certain times of day had higher fluxes than others, but that overall, there was little difference in fluxes at midday versus midnight. Measured EC fluxes revealed no statistically significant difference between paired $CO_2$ fluxes measured during the day (1100 to 1300) as compared to night (2300 to 0100; $p$=0.09; Fig. 4; Table S5), and no statistically significant difference between paired, measured day and night $CH_4$ fluxes ($p$=0.16; Fig. 4; Table S5). We did observe significantly higher median $CO_2$ fluxes measured at dawn (0500 to 0700; 1.34 μmol $m^{-2}$ $s^{-1}$) as compared to dusk (1700 to 1900; -0.030 μmol $m^{-2}$ $s^{-1}$; $p$<0.001; Fig 4; Table S5), which may be related to higher median dawn wind speeds ($p$<0.001), though there was no statistical difference between dawn and dusk $CH_4$ fluxes.

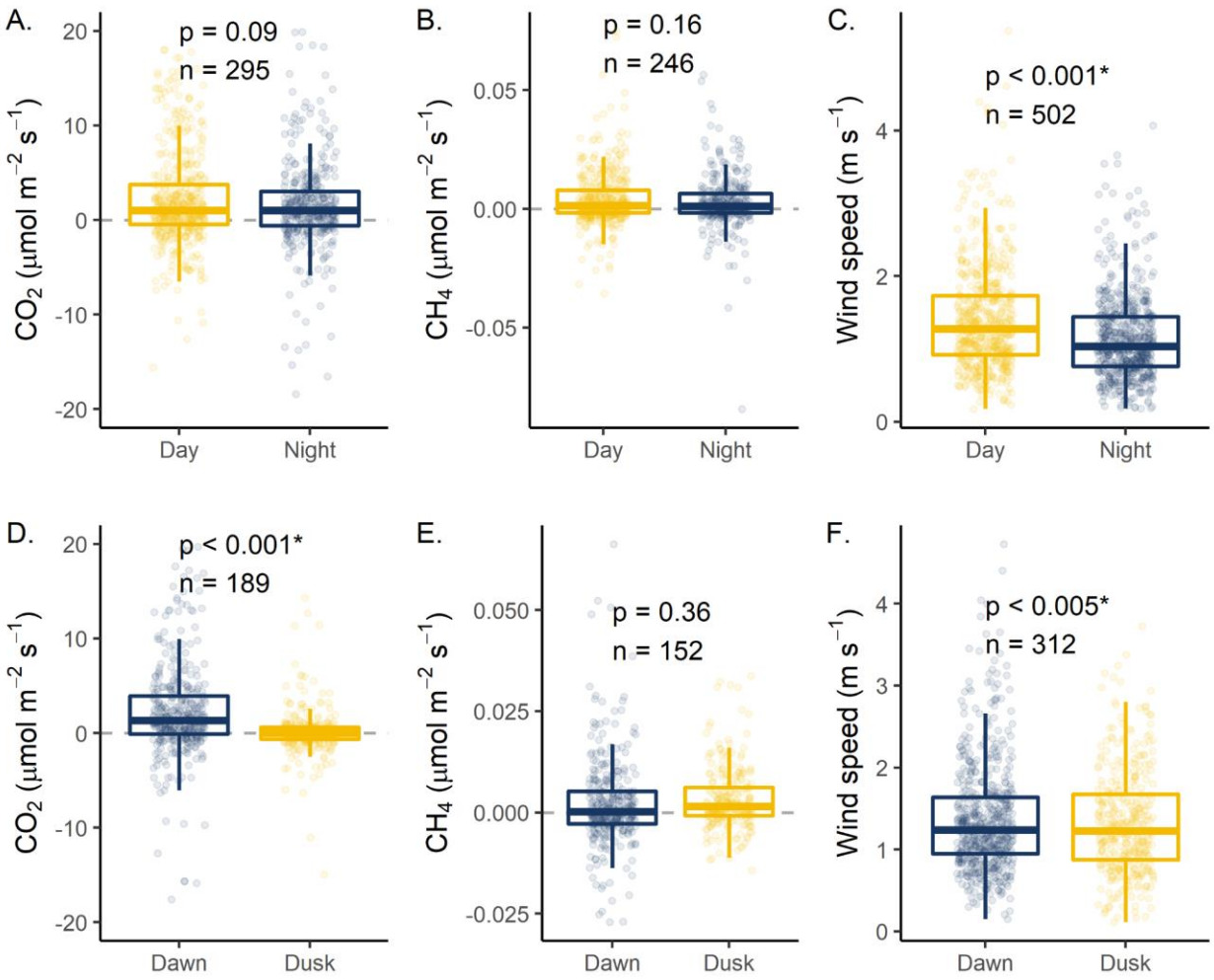


**Figure 4.** Day (1100 to 1300) vs. night (2300 to 0100) comparisons of A. carbon dioxide ($CO_2$, µmol $m^{-2}$ $s^{-1}$), B. methane ($CH_4$, µmol $m^{-2}$ $s^{-1}$), and C. wind speed (m $s^{-1}$) measured using the eddy covariance (EC) system deployed at Falling Creek Reservoir. Points represent measured half-hourly fluxes, while the boxes represent the 25th and 75th percentile, respectively and the thick line shows the median flux calculated with measured EC data. Dawn (0500 to 0700) vs. dusk (1700 to 1900) comparisons of D. $CO_2$, E. $CH_4$, and F. wind speed. Wilcoxon signed-rank tests were used to determine statistical significance between paired (day to night; dawn to dusk) measurements. Statistical significance was defined a priori as $p<0.05$; asterisks indicate statistically significant differences. n indicates the number of paired measurements (Table S5). For $CO_2$ (A. and B.) some outliers were omitted for data presentation but retained for analysis.

At the seasonal scale, both $CO_2$ and $CH_4$ fluxes (EC and diffusive measured fluxes) were greater in magnitude and more variable during the summer than winter, with increasing fluxes during the late spring and decreasing fluxes during the late fall (Figs. 2, 3). During the summer months (June – August), FCR was an overall source of $CO_2$ and $CH_4$ to the atmosphere for both

years (Figs. 2, 3). Specifically, $CO_2$ and $CH_4$ fluxes were up to 5× and 15× greater, respectively, during the summer stratified period (May – October) as compared to the winter and early spring (November – April; Fig. 5, S8). During fall turnover, EC measured $CO_2$ fluxes remained low in both years (2020, 2021), while diffusive fluxes showed an increase in $CO_2$ fluxes on the day of turnover (Figs. 2, S9). Similarly, $CH_4$ fluxes were also low during and following turnover for both EC and diffusive fluxes in both years (Figs. 3, S9). From September to April, FCR was a small $CO_2$ source, but emitted less $CO_2$ than during the summer. For $CH_4$, FCR was almost net neutral from late fall to early spring (November to April), in contrast to larger $CH_4$ emissions during the summer. Following spring mixing, there was a small, but notable increase in $CO_2$ emissions in 2021 but little change in $CH_4$. In 2022, there were no notable changes in either $CO_2$ or $CH_4$ following ice-off and subsequent spring mixing in 2022 (Fig. 6). At the annual scale, there were notably higher $CO_2$ fluxes in the late-summer and early fall 2021 as compared to the summer and fall 2020, while for $CH_4$, there were notably higher fluxes both in the mid-summer 2021 and in the late-summer and early fall 2021 (Figs. 2, 3).

### 3.2 Comparison of EC and diffusive fluxes

Overall, both $CO_2$ and $CH_4$, diffusive fluxes were within the range of measured EC fluxes, though diffusive $CO_2$ fluxes were lower than measured EC fluxes when comparing discrete timepoints (Fig. 2, 3; Table S4). Specifically, hourly $CO_2$ diffusive fluxes calculated from grab surface samples were an order of magnitude lower than measured EC fluxes and ranged from -1.24 to 17.50 μmol $m^{-2}$ $s^{-1}$, with a mean flux of 0.39 ± 1.29 μmol $m^{-2}$ $s^{-1}$ (Figs. 2, S10, S11; Table S4). We note that the magnitude of diffusive fluxes was highly sensitive to the gas transfer coefficient method (k) used in flux calculations, and thus we present the mean and standard deviation of the seven different k methods used (Eq. 1; Fig. S10). Hourly $CH_4$ diffusive fluxes were more comparable to measured EC fluxes, with a range of -0.003 to 0.096 μmol $m^{-2}$ $s^{-1}$ and a mean of 0.006 ± 0.009 μmol $m^{-2}$ $s^{-1}$ (Figs. 3, S10, S11; Table S4).

### 3.3 Net $CO_2$ and $CH_4$ balance for a small, eutrophic reservoir

Gap-filled $CO_2$ and $CH_4$ half-hourly fluxes summed across the entire year indicate that FCR was an overall source of $CO_2$ and $CH_4$ to the atmosphere (Fig. 5). According to gap-filled EC fluxes, FCR released 633 and 731 g $CO_2$-C $m^{-2}$ $year^{-1}$, during the first and second years of the

study, respectively. For gap-filled $CH_4$ fluxes, FCR released 1.02 and 1.29 g $CH_4$-C $m^{-2}$ $year^{-1}$, respectively. The gap-filled and measured data yielded similar estimates when the gap-filled data were scaled by the percentage of missing data from the measured time series (Fig. S12).

The annual GHG balances were driven by large fluxes of $CO_2$ and $CH_4$ during the summer. Net emissions during the warmest months (June – September; 375 and 496 g $CO_2$-C $m^{-2}$ for year 1 and year 2, respectively) represented up to 68% of the total annual net $CO_2$ flux as compared to the coldest months (December – March) when only 98 and 57 g $CO_2$-C $m^{-2}$ was emitted (up to 15% of the total annual $CO_2$). Similarly, for $CH_4$, up to 66% of the total annual net $CH_4$ flux was released during the warmest months (June – September; 0.67 and 0.76 g $CH_4$-C $m^{-2}$) and less than 1% during the coldest months (December – March). For the second year of monitoring, annual fluxes were greater for both $CO_2$ and $CH_4$, largely due to elevated fluxes in early and late fall (September – November). Cumulatively, the amount of $CO_2$-C released from FCR was three orders of magnitude greater than the mass of $CH_4$-C released.

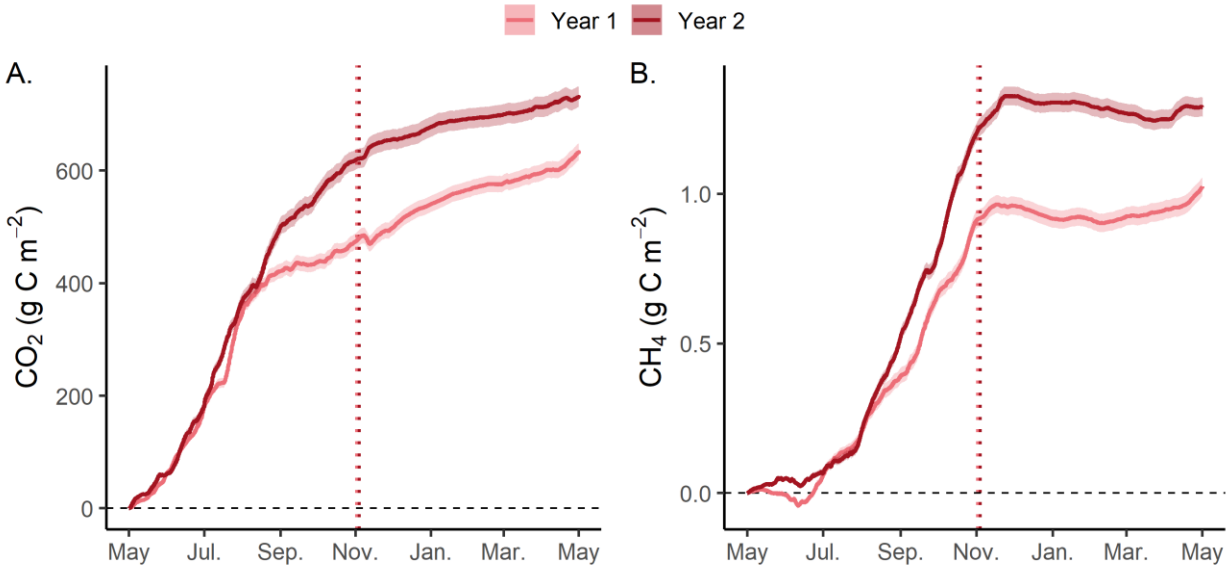


**Figure 5.** Annual cumulative fluxes using measured and gap-filled eddy covariance (EC) data for A. carbon dioxide ($CO_2$, g C $m^{-2}$) and B. methane ($CH_4$, g C $m^{-2}$) using measured and gap-filled EC fluxes from Falling Creek Reservoir for Year 1 (May 2020-April 2021; pink) and Year 2 (May 2021-April 2022; dark red). Shaded areas correspond to the aggregated standard deviation (±1 S.D.) of measurements. The horizontal dashed line corresponds to zero and the vertical dotted line indicates reservoir fall turnover for both years.

### 3.4 Environmental predictors of $CO_2$ and $CH_4$ fluxes

During the study period, FCR experienced typical meteorological and environmental conditions. The meteorology measured at the reservoir dam recorded a mean air temperature of 14.1°C (13.8 and 14.4°C in years 1 and 2, respectively), with a minimum and maximum temperature of -11.5 and 35.1°C, respectively across the two years (Table S6). Mean wind speed during the time period was 1.99 m $s^{-1}$ (2.00 and 1.97 m $s^{-1}$ for years 1 and 2, respectively), with a maximum wind speed of 11.2 m $s^{-1}$ and a dominant wind direction of 198° (191° and 199° for years 1 and 2, respectively). Yearly total rainfall ranged from 790 mm (Year 2) to 1438 mm (Year 1). During the winter (January - February), air temperatures in year 1 ranged from -8.0 to 19.4°C with a mean of 1.9°C and in year 2 ranged from -11.5 to 21.4°C with a mean of 2.1°C.

Water column variables also exhibited typical annual patterns and were for the most part similar between years. We found surface water temperatures ranged from 1.23 to 31.4°C, with a mean of 15.2 and 15.9°C for years 1 and 2, respectively (Fig. S2; Table S7). Chl-a values ranged from 0.25 to 121 μg $L^{-1}$, with a mean of 11.5 μg $L^{-1}$ and 12.3 μg $L^{-1}$ in years 1 and 2, respectively. fDOM was also nearly identical in years 1 and 2 with a mean of 6.09 and 6.04 RFU, respectively, and a range of 3.01 to 10.4 RFU. For DO sat., the mean was 107 and 97.8% in year 1 and year 2. Finally, inflow was higher in year 1 (0.056 $m^3$ $s^{-1}$) as compared to year 2 (0.013 $m^3$ $s^{-1}$) and ranged from 0.005 to 0.27 $m^3$ $s^{-1}$ (Fig. S2; Table S7).

Overall, surface water temperature and thermocline depth were found to be the most important environmental predictors for both $CO_2$ and $CH_4$ fluxes over all timescales analyzed (daily, weekly, monthly), followed by fDOM (Table 1). Inflow discharge was only intermittently important for $CO_2$ and $CH_4$ fluxes at various timescales while DO sat. and Chl-a were only intermittently important for $CO_2$ fluxes (Tables 1, S8). Water temperature was positively correlated with both $CO_2$ and $CH_4$ fluxes at all timescales, following the pattern of higher GHG fluxes during summer as compared to winter in the time series data (Figs. 2, 3). $CO_2$ was negatively associated with thermocline depth while $CH_4$ was positively associated with thermocline depth at all timescales (Table 1); i.e., $CO_2$ fluxes were greater when there were

shallower thermocline depths, whereas $CH_4$ fluxes were greater when there were deeper thermocline depths.

In addition to water temperature and thermocline depth, $CO_2$ was positively associated with fDOM across all timescales, while $CH_4$ was only positively associated with fDOM at the daily and weekly timescales (Table 1). Conversely, inflow was positively associated with $CO_2$ at daily and weekly timescales, while inflow was negatively associated with $CH_4$ at weekly and monthly timescales. Finally, Chl-a was negatively associated with $CO_2$, but only on the daily timescale and was negatively associated with DO sat. at the weekly timescale. $CH_4$ was not associated with either Chl-a or DO sat. at any timescale.

$CO_2$ fluxes were best predicted by ARIMA models at the monthly timescale (RMSE=0.48 μmol $m^{-2}$ $s^{-1}$), with descending RMSE for the weekly (0.63 μmol $m^{-2}$ $s^{-1}$) and then daily (0.97 μmol $m^{-2}$ $s^{-1}$) models (Tables 1; S8). For $CH_4$, the best-fitting ARIMA model was also identified at the monthly timescale (RMSE=0.41 μmol $m^{-2}$ $s^{-1}$), with descending RMSE for the weekly and daily models ranging from 0.64 and-1.02 μmol $m^{-2}$ $s^{-1,}$ respectively (Tables 1, S8). Full ARIMA results are reported in Table S8.

**Table 1.** *Best-fit results from Autoregressive Integrated Moving Average (ARIMA) analysis*

| GHG | Timescale | Model Order | Surface Temp (°C) | DO Sat. (%) | Chl-a (µg $L^{-1}$) | fDOM (RFU) | Inflow ($m^3$ $s^{-1}$) | Thermo. Depth (m) | RMSE (µmol $m^2$ $s^{-1}$) |
|---|---|---|---|---|---|---|---|---|---|
| CO2 | Daily | (1,0,0) | 0.18 | - | -0.17 | 0.07 | 0.08 | -0.09 | 0.97 |
| | Weekly | (0,0,0) | 0.64 | -0.16 | - | 0.13 | 0.20 | -0.19 | 0.63 |
| | Monthly | (0,0,0) | 0.73 | - | - | 0.24 | - | -0.31 | 0.48 |
| CH4 | Daily | (0,0,0) | 0.27 | - | - | 0.12 | - | 0.25 | 1.02 |
| | Weekly | (0,1,1) | 0.36 | - | - | 0.23 | -0.36 | 0.24 | 0.64 |
| | Monthly | (0,0,1) | 0.74 | - | - | - | -0.26 | 0.21 | 0.41 |

*Note:* Table includes only the top selected model (lowest corrected Akaike Information Criterion, AICc). Models are separated by greenhouse gas (GHG) flux as carbon dioxide ($CO_2$) and methane ($CH_4$) as well as by timescale (daily, weekly, monthly). Environmental predictors included: Surface temperature (Surface Temp, °C), dissolved oxygen saturation (DO Sat, %), Chlorophyll-*a* (Chl-*a*, µg $L^{-1}$), fluorescent dissolved organic matter (fDOM, RFU), inflow discharge (Inflow, $m^3$ $s^{-1}$), and thermocline depth (Thermo. Depth, m). Model order is specified as (p,d,q) where p is the order of the AR term, d is the order of the integration term, and q is the order of the MA term. For brevity, the autoregressive (AR) and moving average (MA) terms have been removed but can be found in the supplemental information. Results for all models with 2 AICc of the best fitting model, can be found in the supplemental information (Table S8). Dashed lines indicate environmental parameters that were not identified as statistically significant. The root mean square error (RMSE) is reported for each model. Standard errors for each parameter value are given in Table S8.

### 3.5 Influence of ice cover on $CO_2$ and $CH_4$ fluxes

FCR experienced two distinct winter regimes in 2021 vs. 2022. In 2021, ice-on first occurred on 10 January 2021, then came on and off multiple times before final ice-off on 23 February 2021. Overall, there were 27 days with some ice and 9 days with some open-water during the 2021 intermittent ice-period. In contrast, in 2022, there was near-continuous ice cover from 10 January to 10 February, with ice-on occurring from 16 January 2022 and final ice-off on 10 February 2022. While we were unable to collect ice thickness data through both winters due to safety concerns, peak ice thickness in FCR in 2022 was ~9.5 cm whereas peak ice thickness in 2021 was ~2 cm.

When comparing measured half-hourly fluxes aggregated across the intermittent ice-on period in winter 2021 and the continuous ice-on period in winter 2022, there were statistically-significantly higher median $CO_2$ and $CH_4$ fluxes measured during intermittent ice-on than continuous ice-on (Kruskal-Wallis $p<0.0001$; Fig. 6; Table S9). During intermittent ice-on in winter 2021, median $CO_2$ fluxes were 0.71 μmol $m^{-2}$ $s^{-1}$, 2.5× higher than the median of 0.28 μmol $m^{-2}$ $s^{-1}$ during continuous ice-on in 2022. For $CH_4$, median fluxes were 0.001 μmol $m^{-2}$ $s^{-1}$ and -0.001 μmol $m^{-2}$ $s^{-1}$, during intermittent ice-on and continuous ice-on, respectively (Table S9). Throughout the winter period, mean daily $CO_2$ and $CH_4$ fluxes were much lower and less variable than in the summer, for both years (Fig. 2, 3).

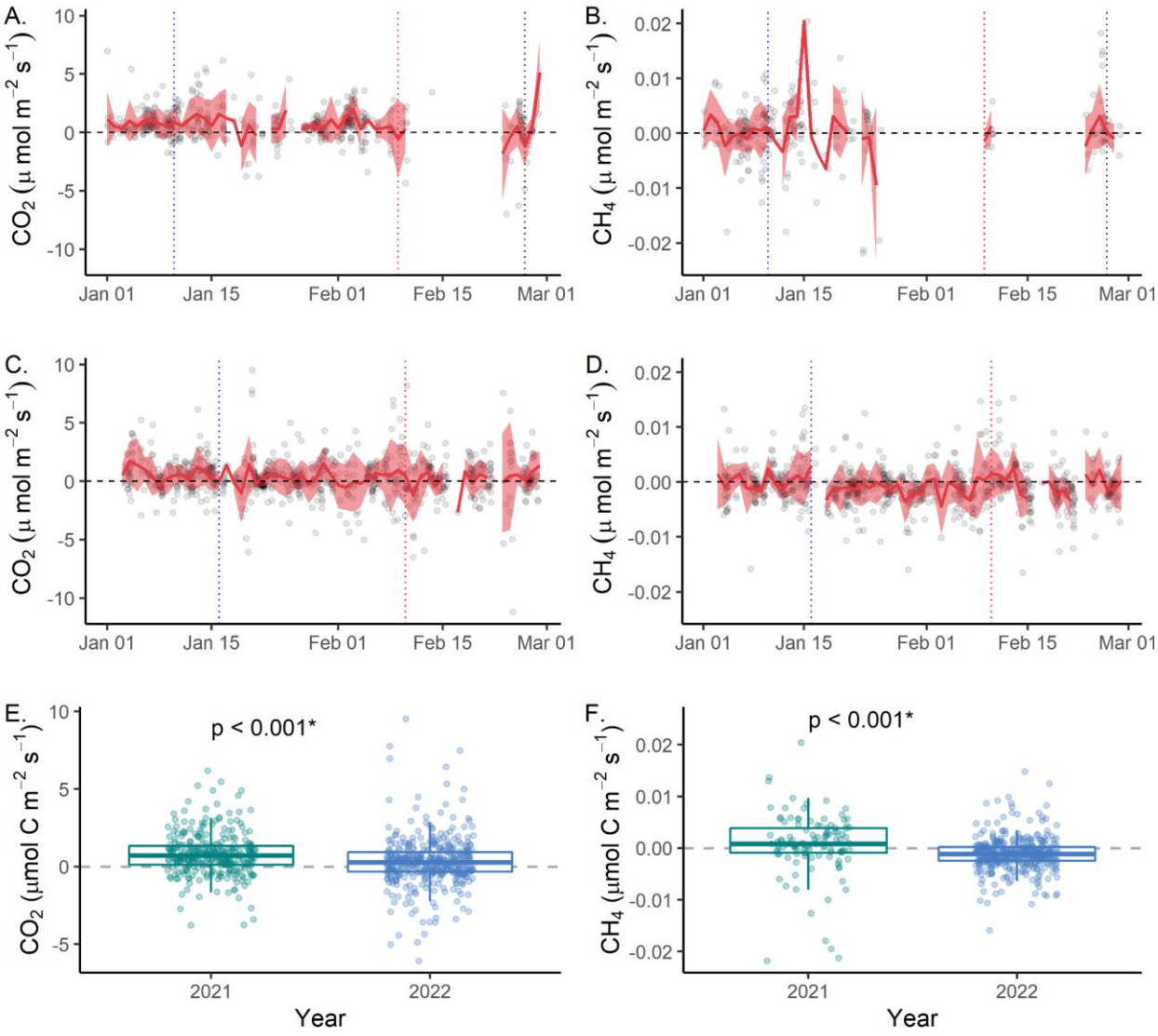


**Figure 6.** Mean daily fluxes during the winter of 2021 for A. Carbon dioxide ($CO_2$, µmol $m^{-2}$ $s^{-1}$) and B. Methane ($CH_4$ µmol $m^{-2}$ $s^{-1}$) during intermittent ice-on. Mean daily fluxes during winter of 2022 for C. $CO_2$ and D. $CH_4$ during continuous ice-on. Grey dots represent measured half-hourly fluxes while the solid red line indicates mean daily fluxes. The shaded red area corresponds to the standard deviation (±1 S.D.) of the daily mean fluxes. The blue vertical dashed lines correspond to the start of either intermittent or continuous ice-on for winter 2021 and 2022, respectively, while the red vertical dashed lines correspond to the start of complete ice-off. The black dashed line in 2021 corresponds to spring mixing (first day after ice-off when the temperature at 1 m and 8 m was < 1°C). For 2022, spring mixing was on the same day as ice-off. Boxplots of measured E. $CO_2$ and F. $CH_4$ fluxes during each winter's intermittent or continuous ice-on, respectively. For each box plot, the median is represented as the bold line while the 25$^{th}$ and 75$^{th}$ percentiles are represented as the bottom and top of the box, respectively. The whiskers represent minimum and maximum values (1.5× interquartile range). Points represent all half hourly fluxes measured during the respective winter intermittent or continuous ice-on, respectively period. The dashed horizontal line corresponds to zero fluxes. Asterisks

indicate statistically significant differences between median half-hourly fluxes measured during intermittent (2021) and continuous (2022) ice-on periods using Mann-Whitney-Wilcoxon tests ($\alpha = 0.05$).

## 4 Discussion

This study provides the first annual-scale, multi-year estimates of both $CH_4$ and $CO_2$ fluxes using an EC system from a small reservoir. While using EC systems in small freshwaters is inherently challenging and contains several limitations, our work reveals variable patterns in both $CH_4$ and $CO_2$ fluxes over sub-daily to seasonal scales. Our study was limited by low levels of measured data, underscoring the need for more accurately quantifying the GHG contributions of small reservoirs on multiple timescales. Despite these challenges, however, our data suggest that FCR was a substantial $CO_2$ and $CH_4$ source to the atmosphere. Below we discuss some of the challenges of using an EC system in small freshwaters as well as the patterns and potential drivers of variability in fluxes ($CO_2$ and $CH_4$) over multiple timescales. We also discuss the role of various environmental parameters in constraining GHGs fluxes, including during winter ice-cover in small, temperate systems.

### 4.1 Variability in sub-daily fluxes, with higher dawn than dusk $CO_2$ fluxes

A key advantage of an EC system is the ability to capture variability in sub-daily GHG fluxes throughout the year. Despite data gaps and limitations, the fluxes collected by the EC represent a substantial increase in the ability to identify variability in fluxes at multiple timescales. Our work complements previous studies of freshwater systems using EC measurements that observed high sub-daily variability in both summer $CO_2$ (Liu et al. 2016; Golub et al. 2021; Shao et al. 2015) and $CH_4$ fluxes (Eugster et al. 2011; Podgrajsek et al. 2014; Taoka et al. 2020; Waldo et al. 2021) and furthers our understanding of the variability of $CO_2$ and $CH_4$ fluxes on multiple timescales.

When comparing day (1100 to 1300) versus night (2300 to 0100) fluxes, we observed no statistically significant differences between $CO_2$ or $CH_4$ fluxes during the day as compared to night using measured EC fluxes aggregated over the full year (Fig. 4). Similarly, studies in two small Finnish lakes also found no evidence for diel differences in $CO_2$ fluxes (Erkkilia et al.

2018; Mammarella et al. 2015), while Waldo et al. (2021) found diel differences in $CH_4$ fluxes on only 18.5% of days out of a 2-year study period. Other studies, however, have observed more consistent diel patterns in GHG fluxes. For example, some studies have shown higher $CH_4$ fluxes during the night in lakes and reservoirs (Eugster et al. 2011; Podgrasjek et al. 2014; Waldo et al. 2021) and higher $CO_2$ fluxes at night in streams (Attenmeyer et al. 2021; Gómez-Gener et al. 2021). On the other hand, some studies observed higher $CH_4$ fluxes during the day as compared to night (Erkkilia et al. 2018; Jammet et al. 2017; Podgrasjek et al. 2016; Sieczko, et al. 2020). Clearly, there is a range of responses to diel variation among lake and reservoir $CO_2$ and $CH_4$ fluxes, and more work is needed to identify when, where, and why lakes and reservoirs may emit differential GHGs during day vs. night.

While we did not observe statistically significant differences between GHG fluxes measured during the day as compared to night, we did observe statistically significantly higher $CO_2$ fluxes at dawn (0500 to 0700) as compared to dusk (1700 to 1900), but no difference in dawn vs. dusk $CH_4$ fluxes (Fig. 4). Similarly, studies conducted in other lakes also found $CO_2$ flux minima during the late afternoon (~1800) and $CO_2$ flux maxima during the early morning (~0600; Liu et al. 2016; Shao et al. 2015), supporting our observations of higher dawn $CO_2$ fluxes. Liu et al. (2016) hypothesized the lower $CO_2$ fluxes observed during the day (~1800) were likely a result of elevated primary productivity during the afternoon, primarily in the summer months, but could have also been due to convective mixing at night.

Altogether, our results provide additional evidence that the time of sample collection has important implications for upscaling freshwater GHG fluxes to longer timescales (Attenmeyer et al. 2021; Gómez-Gener et al. 2021). A previous study conducted in FCR which estimated $CO_2$ and $CH_4$ diffusive fluxes using discrete GHG measurements only collected at ~noon concluded FCR was often a small $CO_2$ sink during the summer stratified period in 2015-2016 (McClure et al. 2018), whereas our diel EC data indicate that FCR was an overall $CO_2$ source throughout the summer in both 2020 and 2021. While the flux magnitudes measured by McClure et al. (2018) were similar to the present study, the overall conclusions were different due to the temporal resolution of sample collection.

### 4.2 Important role of water temperature and thermocline depth in constraining daily, weekly, and monthly $CO_2$ and $CH_4$ fluxes

Following our analysis of $CO_2$ and $CH_4$ fluxes over daily to seasonal timescales, we then used time-series analysis to test the potential effects of various environmental variables on GHG fluxes. Specifically, ARIMA results show that surface water temperature was positively correlated with both $CO_2$ and $CH_4$ fluxes at the daily, weekly, and monthly timescales (Table 1). These results were supported by higher fluxes of both $CO_2$ and $CH_4$ observed during the warmer summer months when aggregated to daily, weekly, and monthly timescales (Fig. 2, 3, S7). Strong positive correlations between GHG fluxes (both $CO_2$ and $CH_4$) and water temperature have been observed in several freshwater ecosystems, especially on longer timescales, with clear differences between summer and winter fluxes (monthly to seasonally; Eugster et al. 2011; Reed et al. 2018; Taoka et al. 2020).

In addition to temperature, thermocline depth was also identified as an important environmental parameter controlling both $CO_2$ and $CH_4$ fluxes. For $CO_2$, thermocline depth was negatively associated with fluxes at all timescales, indicating higher $CO_2$ fluxes when the thermocline was shallower. Generally, thermocline depth was shallower in the late summer (Fig. S3) when $CO_2$ fluxes were observed to be greatest and most variable in FCR. This pattern may be indirectly related to water temperature, as shallower thermocline depths were weakly negatively associated with warmer water temperatures, and there was a strong positive relationship between $CO_2$ fluxes and water temperature, as discussed above.

Conversely, thermocline depth was positively correlated with $CH_4$ at all timescales (daily, weekly, monthly), indicating higher $CH_4$ fluxes when the thermocline depth was deeper, which was generally observed during the late spring and early summer (Fig. S3). Previous studies have suggested water column mixing is an important control on $CH_4$ fluxes, leading to higher fluxes during convective and wind-driven mixing when high concentrations of $CH_4$ accumulated in the deeper waters are mixed to the surface, which would be more common when the thermocline depth is deeper (Sieczko et al. 2021). In addition, we hypothesize this relationship may also be due to the contribution of ebullition to total $CH_4$ fluxes, which has shown to be a small but important component of $CH_4$ fluxes near the deepest point of FCR,

where the EC system was deployed (McClure et al. 2020). We might expect ebullition to provide a greater percentage of overall emissions when the thermocline is deeper, though additional research is needed to confirm this mechanism.

Following temperature and thermocline depth, fDOM was identified as a key positive environmental predictor for $CO_2$ fluxes at all timescales (daily, weekly, monthly; Table 1). A similar positive relationship between terrestrially-derived DOM and dissolved $CO_2$ was identified in 48 Canadian streams (D'Amario and Xenopoulos, 2015). As fDOM sensors are thought to mainly capture allochthonous DOM (Howard et al. 2021; Watras et al. 2015), this finding suggests that allochthonous DOM from the reservoir's primary inflow stream or diffuse overland flow may result in elevated $CO_2$ emissions from freshwater ecosystems. This follows previous research which has identified allochthonous carbon inputs and associated DOC concentrations as important predictors of $CO_2$ fluxes in lakes (Sobek et al. 2005). Unlike for $CO_2$, fDOM was only identified as an important environmental predictor for $CH_4$ fluxes at shorter timescales (daily, weekly). In an analysis of >300 lakes, Sanches et al. (2019) found a strong positive relationship between dissolved organic C and diffusive $CH_4$ fluxes, suggesting dissolved organic C may play an important role in constraining $CH_4$ fluxes across multiple lakes and timescales. The strong positive correlation between $CH_4$ fluxes and fDOM observed here further indicates that dissolved organic C, as a proxy from fDOM (Howard et al. 2021), may also be important at the local scale on short-timescales.

In addition to these overarching patterns, several environmental parameters were intermittently important for various timescales for either $CO_2$ or $CH_4$. $CO_2$ was positively correlated with inflow at shorter timescales (daily, weekly) while $CH_4$ was negatively correlated with inflow but only at longer timescales (weekly, monthly; Table 1). Following the positive relationship between $CO_2$ and fDOM, we hypothesize the positive relationship with inflow reflects the importance of allochthonous DOM delivery to FCR via the primary inflow and diffuse overland flow. Previous research examining $CH_4$ fluxes from FCR have found similar negative relationships between inflow and $CH_4$ fluxes, especially via ebullition in the upstream, littoral portion of the reservoir (McClure et al. 2020). Results from this study suggest inflow is similarly correlated with $CH_4$ fluxes at the deepest point of the reservoir, primarily on longer timescales (weekly, monthly). Finally, Chl-a was negatively associated with $CO_2$ fluxes at the

daily timescale while DO sat. was negatively associated with $CO_2$ fluxes at the weekly timescale (Table 1). Both of these relationships suggest a coupling between high primary production, as indicated by high Chl-a and high DO Sat., and low $CO_2$ fluxes on shorter timescales (daily, weekly). Previous studies have identified a weak negative relationship between primary production and $CO_2$ fluxes on the sub-daily timescale in other eutrophic, freshwater lakes and reservoirs (Liu et al. 2016; Shao et al. 2015).

### 4.3 Role of fall turnover and ice cover in affecting GHG dynamics

Contrary to previous studies conducted in both FCR and other thermally-stratified waterbodies (e.g., Erkkilia et al. 2018; McClure et al. 2018; 2020), we observed low $CO_2$ and $CH_4$ fluxes during the days surrounding fall turnover for both years (1 November 2020; 3 November 2021), when EC data indicate that FCR was a small to negligible $CO_2$ and $CH_4$ source (Fig. 2, 3, S9). Discrete diffusive fluxes measured on the day of fall turnover suggest FCR was a 4x and 14x larger $CO_2$ source than fluxes measured with the EC, in years 1 and 2 (Figs. 2, S9). Similar to $CO_2$, we found the magnitude of $CH_4$ fluxes decreased following fall turnover but remained a small source (Fig. 3, S9). McClure et al. (2018) observed episodic release of $CH_4$ from FCR during the weeks prior to fall turnover as high concentrations of $CH_4$ that had accumulated in the middle of the water column were emitted during wind-mixing. In the weeks prior to fall turnover, we did observe elevated $CH_4$ emissions in both years (Figs. 3, S9), supporting this observed mechanism (McClure et al. 2018), and decreasing the importance of fall turnover as a single pulse of emissions.

Importantly, this study provides some of the first near-continuous flux measurements of both $CO_2$ and $CH_4$ during winter, including during intermittent and continuous ice-on conditions (Fig. 6). We found significantly higher $CO_2$ and $CH_4$ fluxes during intermittent ice-on as compared to continuous ice-on ($p<0.001$; Fig. 6; Table S9), demonstrating the importance of annually-variable, winter ice dynamics to seasonal GHG fluxes. Of the studies that report GHG fluxes during continuous ice-on, all report low fluxes with low variability (A.K. Baldocchi et al. 2020; Jammet et al. 2015, 2017; Reed et al. 2018), similar to the winter with continuous ice-on at FCR. Interestingly, these studies also noted high fluxes immediately following ice-off for both $CO_2$ and $CH_4$ (Anderson et al. 1999; A.K. Baldocchi et al. 2020; Gorsky et al. 2021; Jammet et

al. 2015, 2017; Podgrajsek et al. 2015; Takoa et al. 2020), which was not observed at FCR. Unlike these previous studies, which were largely conducted in northern lakes which are frozen for months at a time, FCR is a more temperate system which only periodically freezes for a few days to months at time (Carey and Breef-Pilz, 2022). We hypothesize that the brief continuous ice-cover observed at FCR during winter 2022 (25 days) was not long enough to promote extensive accumulation of GHGs under ice, as observed by the other studies. Further work on the effect of ice cover on GHG fluxes is needed, but our comparison of intermittent ice-on vs. continuous ice-on suggests that the increasing intermittent ice-cover being experienced in many lakes worldwide (Imrit and Sharma, 2021; Sharma et al. 2021; Woolway et al. 2020) will likely increase winter GHG fluxes.

### 4.4 Much higher annual $CO_2$ emissions from FCR than other studied reservoirs

When scaling fluxes to the full year, FCR was a much smaller annual $CH_4$ source (1.02-1.29 g $m^{-2}$ $yr^{-1}$), yet a larger $CO_2$ source (633-731 g $m^{-2}$ $yr^{-1}$; Figs. 5, S12), than other reservoirs reported in the literature to date (A.K. Baldocchi et al. 2020; Deemer et al. 2016; Golub et al. 2021). While the total magnitude of $CO_2$ emissions from FCR was greater than most studies, Golub et al. (2021) similarly found that data from 12 lakes and reservoirs over multiple years emitted substantial amounts of $CO_2$ in their synthesis of EC measured $CO_2$ fluxes in freshwaters (13.6 - 224 g C $m^{-2}$ $yr^{-1}$), except for one reservoir during one year which had a $CO_2$ flux of -53.6 g C $m^{-2}$ $yr^{-1}$. As compared to other reservoirs with GHG flux data, FCR is old (>100 years old) which may lead to lower GHG emissions, particularly $CH_4$ (Barros et al. 2011; McClure et al. 2020; Prairie et al. 2018).

Despite its age, however, FCR was a much larger $CO_2$ source as compared to other lakes and reservoirs. The $CO_2$ emissions were consistently high among years, suggesting that FCR may be a greater source of $CO_2$ than most terrestrial environments (-70 to 20 g C $m^{-2}$ $yr^{-1}$ for multi-year, undisturbed terrestrial sites; D.D. Baldocchi et al. 2020). Comparisons between years suggest that slightly higher annual fluxes of $CO_2$ and $CH_4$ in the early to late fall (September - November) of the first monitoring year as compared to the second year may be related to slightly higher mean air temperatures or lower inflow levels (and corresponding longer hydraulic residence times), though this remains unknown. We note that these cumulative fluxes are likely

conservative, as there were substantial gaps in measured EC fluxes during year 1, particularly in August 2020, likely resulting in underestimated measured fluxes during this time of year when fluxes are usually highest (Fig. 5, S12).

### 4.5 Challenges of using EC systems in small, freshwater lakes and reservoirs

While the study described here greatly expands the temporal frequency of measured $CO_2$ and $CH_4$ fluxes from a small reservoir, several caveats must be taken into consideration. EC systems are notoriously difficult to use in freshwater ecosystems due to footprint considerations (Vesala et al. 2006), frequent occurrences of low u* values, particularly at night (Vesala et al. 2006; Scholz et al. 2021), as well as general considerations resulting in high percentages of data removed due to these and other issues (yielding data coverage of 10 – 40%; e.g., A.K. Baldocchi et al. 2020; Erkkilia et al. 2018; Houtari et al. 2011; Ouyang et al. 2017; Shao et al. 2015; Waldo et al. 2021; Table S3). While low data coverage is common, data gaps were relatively consistent across timescales (daily to seasonally) to ensure unbiased data. Furthermore, compared to the temporal frequency of many grab sample methods (i.e., samples measured weekly, biweekly, or monthly), the data coverage of the EC system is still a substantial improvement and more accurately captures fluxes across multiple timescales challenging to sample, such as at night, during winter ice-cover, and during episodic events, such as fall turnover.

While strict filtering processes were enacted to limit non-local fluxes (i.e., filtering fluxes when the along-wind distance providing 90% of the cumulative contribution was outside the reservoir), we are unable to completely rule out potential non-local processes (e.g., land-lake interactions) which occur outside the footprint and are entrained or advected into the EC footprint area (Esters et al. 2020; Vesala et al. 2006, 2011; Fig. S1). These processes may be particularly important in small freshwaters located in mountainous regions (Scholz et al. 2021). Based on studies conducted in similar terrestrial ecosystems, we might expect negative $CO_2$ fluxes in the summer followed by substantial $CO_2$ emissions in the fall and winter; however, these patterns were not observed in FCR, suggesting the majority of fluxes measured in this study likely originated in the reservoir. When taken into account and interpreted cautiously, the data collected by the EC system provides a far more comprehensive time series than what is possible from discrete measurements (Anderson et al. 1999; Eugster 2003; Houtari et al. 2011;

749 Jonsson et al. 2008; Scholz et al. 2021), which is critical for increasing our understanding of
750 GHG fluxes from small reservoirs on multiple temporal scales.

751 Finally, comparisons with diffusive grab samples suggest fluxes measured with the EC
752 system were consistently higher than those estimated with diffusive grab samples, especially for
753 $CO_2$ (Fig 2, S11), which is consistent with previous studies (Scholz et al. 2021, and references
754 therein). Conversely, $CH_4$ fluxes calculated using the discrete diffusive methods were more
755 comparable to those measured by the EC system (Fig. 3, S11). Discrepancies between EC
756 measured fluxes and diffusive grab samples may be a result of the different spatial resolution of
757 the two methods, where the EC system is measuring fluxes both at the deepest point of the
758 reservoir in addition to upstream and littoral portions of the reservoir while diffusive grab
759 samples were only collected at the deepest point of the reservoir (Fig. 1; Scholz et al. 2021).
760 Indeed, several studies have observed higher $CO_2$ and $CH_4$ fluxes in the littoral zone, closer to
761 the shore, which would have been encompassed in the measured EC fluxes but not the diffusive
762 grab samples (Erkkilia et al. 2018; McClure et al. 2020; Scholz et al. 2021; Taoka et al. 2020),
763 though additional studies in FCR are needed to confirm this pattern.

764

765 **5 Conclusions**

766 Overall, we observed FCR to be a source of $CO_2$ and $CH_4$ to the atmosphere on annual
767 timescales (633-731 g $CO_2$-C $m^{-2}$ $yr^{-1}$; ~1.02-1.29 g $CH_4$-C $m^{-2}$ $yr^{-1}$). Importantly, by measuring
768 fluxes near-continuously for a full year, we found winter fluxes (December-March) of both $CO_2$
769 and $CH_4$ to be comparatively smaller (15-25% and <1% of total annual fluxes, respectively) than
770 the summer stratified period (June - September) yet still important for annual GHG fluxes. In
771 addition, measuring GHG fluxes during two winters with contrasting ice-cover, showed
772 significantly higher $CO_2$ and $CH_4$ fluxes during intermittent as compared to continuous ice-on.
773 Finally, we identified surface water temperature, thermocline depth, and several other
774 environmental variables (fDOM, inflow) as important drivers of both $CO_2$ and $CH_4$ fluxes on
775 multiple timescales. Altogether, our results suggest that $CO_2$ and $CH_4$ are highly dynamic on

multiple temporal scales and highlight the role of small reservoirs as important GHG sources in global budgets.

## Acknowledgments

This project originated in February 2020 and was made possible through creative teamwork spanning international borders amidst a global pandemic. We thank Bobbie Niederlehner, Bethany Bookout, Heather Wander, Abigail Lewis, Whitney Woelmer, Dexter Howard, Nicholas Hammond, Arpita Das, Ryan McClure, Mary Lofton, and Calvin Thomas for their assistance with field collection and laboratory analysis. Zoran Nesic and Vahid Daneshmand provided critical troubleshooting assistance and technical support. Additionally, we thank the Western Virginia Water Authority (WVWA), especially Jamie Morris, for long-term access to field sites and logistical support. We gratefully acknowledge funding from U.S. National Science Foundation grants CNS-1737424, DEB-1753639, DEB-1926050, DBI-1933102, and DBI-1933016; and Fralin Life Sciences Institute at Virginia Tech. We also acknowledge Discovery Grant support to Johnson provided by the Natural Sciences and Engineering Research Council of Canada (NSERC), RGPIN-2020-06252. The authors report no conflicts of interest.

## Open Research

The eddy covariance dataset and associated QA/QC code for this study can be found in the Environmental Data Initiative (EDI) repository via https://doi.org/10.6073/pasta/a1324bcf3e1415268996ba867c636489 and https://portal-s.edirepository.org/nis/mapbrowse?packageid=edi.920.2 (Carey et al. 2022a). Additionally, code used for the timeseries and ARIMA analyses are archived at https://10.5281/zenodo.6818141 (Zenodo; Hounshell et al. 2022). Additional datasets including the meteorological data set (https://portal-s.edirepository.org/nis/mapbrowse?scope=edi&identifier=143&revision=14, Carey et al. 2022c), limnological dataset (https://doi.org/10.6073/pasta/81c6c76f4fe22434a20aa8c00f2d4ad1 and https://portal-s.edirepository.org/nis/mapbrowse?scope=edi&identifier=518&revision=11, Carey et al. 2022d),

inflow discharge (https://doi.org/10.6073/pasta/c65755d4c0102dde6e3140c1c91b77d6 and https://portal-s.edirepository.org/nis/mapbrowse?packageid=edi.923.1, Carey et al. 2022e), ice-cover (https://portal.edirepository.org/nis/mapbrowse?packageid=edi.456.4, Carey and Breef-Pilz, 2022), and dissolved discrete grab greenhouse gas concentrations (https://doi.org/10.6073/pasta/2fb836492aace4c13b7962f2718be8e5 and https://portal-s.edirepository.org/nis/mapbrowse?scope=edi&identifier=928&revision=3, Carey et al. 2022b) are also archived in the EDI. All data (2020-2022) are available for review in the EDI staging environment and will be published following manuscript acceptance. All data through 2021 have been published to EDI and are available under the Creative Commons License - Attribution.

## References


Anderson, D.E., Striegl, R.G., Stannard, D.I., Michmerhuizen, C.M., McConnaughey, T.A., & LaBaugh, J.W. (1999). Estimating lake-atmosphere $CO_2$ exchange. *Limnology and Oceanography*, *44*(4), 988–1001. https://doi.org/10.4319/lo.1999.44.4.0988

Attermeyer, K., Casas-Ruiz, J.P., Fuss, T., Pastor, A., Cauvy-Fraunié, S., Sheath, D., et. al. (2021). Carbon dioxide fluxes increase from day to night across European streams. *Communications Earth & Environment*, *2*(1), 118. https://doi.org/10.1038/s43247-021-00192-w

Baldocchi, A.K., Reed, D.E., Loken, L.C., Stanley, E.H., Huerd, H., & Desai, A.R. (2020). Comparing spatial and temporal variation in lake-atmosphere carbon dioxide fluxes using multiple methods. *Journal of Geophysical Research: Biogeosciences*, *125*(12). https://doi.org/10.1029/2019JG005623

Baldocchi, D.D. (2020). How eddy covariance flux measurements have contributed to our understanding of Global Change Biology. *Global Change Biology*, *26*(1), 242–260. https://doi.org/10.1111/gcb.14807

Barros, N., Cole, J.J., Tranvik, L.J., Prairie, Y.T., Bastviken, D., Huszar, V.L.M., del Giorgio, P., & Roland, F. (2011). Carbon emission from hydroelectric reservoirs linked to reservoir age and latitude. *Nature Geoscience*, *4*(9), 593–596. https://doi.org/10.1038/ngeo1211

Bartosiewicz, M., Przytulska, A., Lapierre, J., Laurion, I., Lehmann, M.F., & Maranger, R. (2019). Hot tops, cold bottoms: Synergistic climate warming and shielding effects increase carbon burial in lakes. *Limnology and Oceanography Letters*, *4*(5), 132–144. https://doi.org/10.1002/lol2.10117

Bastviken, D., Sundgren, I., Natchimuthu, S., Reyier, H., & Gålfalk, M. (2015). Technical Note: Cost-efficient approaches to measure carbon dioxide ($CO_2$) fluxes and concentrations in terrestrial and aquatic environments using mini loggers. *Biogeosciences*, *12*(12), 3849–3859. https://doi.org/10.5194/bg-12-3849-2015

Bastviken, D., Tranvik, L.J., Downing, J.A., Crill, P.M., & Enrich-Prast, A. (2011). Freshwater Methane Emissions Offset the Continental Carbon Sink. *Science*, *331*(6013), 50–50. https://doi.org/10.1126/science.1196808

Beaulieu, J.J., DelSontro, T., & Downing, J.A. (2019). Eutrophication will increase methane emissions from lakes and impoundments during the 21st century. *Nature Communications*, *10*(1), 1375. https://doi.org/10.1038/s41467-019-09100-5

Burba, G., Schmidt, A., Scott R.L., Nakai, T., Kathilankal, J., Fratini, G., et al. (2012). Calculating $CO_2$ and $H_2O$ eddy covariance fluxes from an enclosed gas analyzer using an instantaneous mixing ratio. Global Change Biology, *18*(1), 385-399. https://doi.org/10.1111/j.1365-2486.2011.02536.x

Burnham, K.P., & Anderson, D.R. (2002). *Model selection and multimodel inference: a practical information-theoretic approach*. New York, NY: Springer.

Butman, D., Stackpoole, S., Stets, E., McDonald, C.P., Clow, D.W., & Striegl, R.G. (2016). Aquatic carbon cycling in the conterminous United States and implications for terrestrial carbon accounting. *Proceedings of the National Academy of Sciences*, *113*(1), 58–63. https://doi.org/10.1073/pnas.1512651112

Carey, C.C. & Breef-Pliz, A. (2022). Ice cover data for Falling Creek Reservoir, Vinton, Virginia, USA for 2013-2022. (Version 4). [Dataset]. Environmental Data Initiative (EDI). https://portal.edirepository.org/nis/mapbrowse?packageid=edi.456.4

Carey, C.C., Breef-Pilz, A. & Bookout, B.J. (2022c). Time series of high-frequency meteorological data at Falling Creek Reservoir, Virginia, USA 2015-2021 (Version 14). [Dataset]. Environmental Data Initiative (EDI). https://portal-s.edirepository.org/nis/mapbrowse?scope=edi&identifier=143&revision=14

Carey, C.C., Breef-Pilz, A., Hounshell, A.G., Lofton, M.E., McClure, R.P., Gerling, A.B., & Woelmer, W.M. (2022e). Discharge time series for the primary inflow tributary entering Falling Creek Reservoir, Vinton, Virginia, USA 2013-2021. (Version 8). [Dataset].

Environmental Data Initiative (EDI). https://doi.org/10.6073/pasta/c65755d4c0102dde6e3140c1c91b77d6

Carey, C.C., Breef-Pilz, A., Woelmer, W.M., & Bookout, B.J. (2022d). Time series of high-frequency sensor data measuring water temperature, dissolved oxygen, pressure, conductivity, specific conductance, total dissolved solids, chlorophyll a, phycocyanin, and fluorescent dissolved organic matter at discrete depths in Falling Creek Reservoir, Virginia, USA in 2018-2021. (Version 6). [Dataset]. Environmental Data Initiative (EDI). https://doi.org/10.6073/pasta/81c6c76f4fe22434a20aa8c00f2d4ad1

Carey, C.C., Hounshell, A.G., D'Acunha, B.M., Breef-Pilz, A., Thomas, R.Q., & Johnson, M.S. (2022a). Time series of carbon dioxide and methane fluxes measured with eddy covariance for Falling Creek Reservoir in southwestern Virginia, USA during 2020-2022. (Version 1). [Dataset]. Environmental Data Initiative (EDI). https://doi.org/10.6073/pasta/a1324bcf3e1415268996ba867c636489

Carey, C.C., Hounshell, A.G., McClure, R.P., Gerling, A.B., Lewis, A.S.L., & Niederlehner, B.R. (2022b). Time series of dissolved methane and carbon dioxide concentrations for Falling Creek Reservoir and Beaverdam Reservoir in southwestern Virginia, USA during 2015-2021. (Version 6). [Dataset]. Environmental Data Initiative (EDI). https://doi.org/10.6073/pasta/2fb836492aace4c13b7962f2718be8e5

Cole, J.J., & Caraco, N.F. (1998). Atmospheric exchange of carbon dioxide in a low-wind oligotrophic lake measured by the addition of $SF_6$. *Limnology and Oceanography*, *43*(4), 647–656. https://doi.org/10.4319/lo.1998.43.4.0647

Cole, J.J., Prairie, Y.T., Caraco, N.F., McDowell, W.H., Tranvik, L.J., Striegl, R.G., et. al. (2007). Plumbing the Global Carbon Cycle: Integrating Inland Waters into the Terrestrial Carbon Budget. *Ecosystems*, *10*(1), 172–185. https://doi.org/10.1007/s10021-006-9013-8

Crusius, J., & Wanninkhof, R. (2003). Gas transfer velocities measured at low wind speed over a lake. *Limnology and Oceanography*, *48*(3), 1010–1017. https://doi.org/10.4319/lo.2003.48.3.1010

D'Amario, S.C., & Xenopoulos, M.A. (2015). Linking dissolved carbon dioxide to dissolved organic matter quality in streams. *Biogeochemistry*, *126*(1–2), 99–114. https://doi.org/10.1007/s10533-015-0143-y

Deemer, B.R., Harrison, J.A., Li, S., Beaulieu, J.J., DelSontro, T., Barros, et. al. (2016). Greenhouse Gas Emissions from Reservoir Water Surfaces: A New Global Synthesis. *BioScience*, *66*(11), 949–964. https://doi.org/10.1093/biosci/biw117

Deemer, B.R., & Holgerson, M.A. (2021). Drivers of Methane Flux Differ Between Lakes and Reservoirs, Complicating Global Upscaling Efforts. *Journal of Geophysical Research: Biogeosciences*, *126*(4). https://doi.org/10.1029/2019JG005600

DelSontro, T., del Giorgio, P.A., & Prairie, Y.T. (2018). No Longer a Paradox: The Interaction Between Physical Transport and Biological Processes Explains the Spatial Distribution of Surface Water Methane Within and Across Lakes. *Ecosystems*, *21*(6), 1073–1087. https://doi.org/10.1007/s10021-017-0205-1

Erkkilä, K.M., Ojala, A., Bastviken, D., Biermann, T., Heiskanen, J.J., Lindroth, A., et. al. (2018). Methane and carbon dioxide fluxes over a lake: Comparison between eddy covariance, floating chambers and boundary layer method. *Biogeosciences*, *15*(2), 429–445. https://doi.org/10.5194/bg-15-429-2018

Esters, L., Rutgersson, A., Nilsson, E., & Sahlée, E. (2021). Non-local Impacts on Eddy-Covariance Air–Lake $CO_2$ Fluxes. *Boundary-Layer Meteorology*, *178*(2), 283–300. https://doi.org/10.1007/s10546-020-00565-2

Eugster, W. (2003). $CO_2$ exchange between air and water in an Arctic Alaskan and midlatitude Swiss lake: Importance of convective mixing. *Journal of Geophysical Research*, *108*(D12), 4362. https://doi.org/10.1029/2002JD002653

Eugster, W., DelSontro, T., & Sobek, S. (2011). Eddy covariance flux measurements confirm extreme CH<sub>4</sub> emissions from a Swiss hydropower reservoir and resolve their short-term variability. *Biogeosciences*, *8*(9), 2815–2831. https://doi.org/10.5194/bg-8-2815-2011

Gash, J.H.C., & Culf, A.D. (1996). Applying a linear detrend to eddy correlation data in realtime. *Boundary Layer Meteorology*, *79*, 301-306. https://doi.org/10.1007/BF00119443

Gerling, A.B., Munger, Z.W., Doubek, J.P., Hamre, K.D., Gantzer, P.A., Little, J.C., & Carey, C.C. (2016). Whole-Catchment Manipulations of Internal and External Loading Reveal the Sensitivity of a Century-Old Reservoir to Hypoxia. *Ecosystems*, *19*(3), 555–571. https://doi.org/10.1007/s10021-015-9951-0

Golub, M., Desai, A.R., Vesala, T., Mammarella, I., Ojala, A., Bohrer, G., et. al. (2021). *New insights into diel to interannual variation in carbon dioxide emissions from lakes and reservoirs* [Preprint]. Environmental Sciences. https://doi.org/10.1002/essoar.10507313.1

Gómez-Gener, L., Rocher-Ros, G., Battin, T., Cohen, M.J., Dalmagro, H.J., Dinsmore, K.J., et. al. (2021). Global carbon dioxide efflux from rivers enhanced by high nocturnal emissions. *Nature Geoscience*, *14*(5), 289–294. https://doi.org/10.1038/s41561-021-00722-3

Gorsky, A.L., Lottig, N.R., Stoy, P.C., Desai, A.R., & Dugan, H.A. (2021). The Importance of Spring Mixing in Evaluating Carbon Dioxide and Methane Flux From a Small North-Temperate Lake in Wisconsin, United States. *Journal of Geophysical Research: Biogeosciences*, *126*(12). https://doi.org/10.1029/2021JG006537

Hanson, P.C., Pace, M.L., Carpenter, S.R., Cole, J.J., & Stanley, E.H. (2015). Integrating Landscape Carbon Cycling: Research Needs for Resolving Organic Carbon Budgets of Lakes. *Ecosystems*, *18*(3), 363–375. https://doi.org/10.1007/s10021-014-9826-9

Heiskanen, J.J., Mammarella, I., Haapanala, S., Pumpanen, J., Vesala, T., MacIntyre, S., & Ojala, A. (2014). Effects of cooling and internal wave motions on gas transfer coefficients in a boreal lake. *Tellus B: Chemical and Physical Meteorology*, *66*(1), 22827. https://doi.org/10.3402/tellusb.v66.22827

Hounshell, A.G. (2022, July 11). aghounshell/EddyFlux: EddyFlux: Hounshell et al. 20XX re-submission (Version 2.0.0). [Software] Zenodo. https://doi.org/10.5281/zenodo.6818141

Howard, D.W., Hounshell, A.G., Lofton, M.E., Woelmer, W.M., Hanson, P.C., & Carey, C.C. (2021). Variability in fluorescent dissolved organic matter concentrations across diel to seasonal time scales is driven by water temperature and meteorology in a eutrophic reservoir. *Aquatic Sciences*, *83*(2), 30. https://doi.org/10.1007/s00027-021-00784-w

Huotari, J., Ojala, A., Peltomaa, E., Nordbo, A., Launiainen, S., Pumpanen, J., et. al. (2011). Long-term direct $CO_2$ flux measurements over a boreal lake: Five years of eddy covariance data: $CO_2$ Fluxes of a boreal lake. *Geophysical Research Letters*, *38*(18). https://doi.org/10.1029/2011GL048753

Hyndman, R.J. & Athanasopoulos, G. (2018). *Forecasting: principles and practice*, 2nd Edition. Otexts, Melbourne, Australia.

Hyndman, R., Athanasopoulos, G., Bergmeir, C., Caceres, G., Chhay, L., O'Hara-Wild, M., et al. (2022, January 10). forecast: Forecasting functions for time series and linear models. (Version 8.16). [Software]. R Package. https://pkg.robjhyndman.com/forecast/

Hyndman, R. J., & Khandakar, Y. (2008). Automatic Time Series Forecasting: The **forecast** Package for *R*. *Journal of Statistical Software*, *27*(3). https://doi.org/10.18637/jss.v027.i03

Imrit, M.A., & Sharma, S. (2021). Climate Change is Contributing to Faster Rates of Lake Ice Loss in Lakes Around the Northern Hemisphere. *Journal of Geophysical Research: Biogeosciences*, *126*(7). https://doi.org/10.1029/2020JG006134

Jammet, M., Crill, P., Dengel, S., & Friborg, T. (2015). Large methane emissions from a subarctic lake during spring thaw: Mechanisms and landscape significance: Lake methane emissions among spring thaw. *Journal of Geophysical Research: Biogeosciences*, *120*(11), 2289–2305. https://doi.org/10.1002/2015JG003137

Jammet, M., Dengel, S., Kettner, E., Parmentier, F.J.W., Wik, M., Crill, P., & Friborg, T. (2017). Year-round $CH_4$ and $CO_2$ flux dynamics in two contrasting freshwater ecosystems of the subarctic. *Biogeosciences*, *14*(22), 5189–5216. https://doi.org/10.5194/bg-14-5189-2017

Jonsson, A., Åberg, J., Lindroth, A., & Jansson, M. (2008). Gas transfer rate and $CO_2$ flux between an unproductive lake and the atmosphere in northern Sweden: $CO_2$ emission in an unproductive lake. *Journal of Geophysical Research: Biogeosciences*, *113*(G4). https://doi.org/10.1029/2008JG000688

Klaus, M., Seekell, D.A., Lidberg, W., & Karlsson, J. (2019). Evaluations of Climate and Land Management Effects on Lake Carbon Cycling Need to Account for Temporal Variability in CO $_2$ Concentrations. *Global Biogeochemical Cycles*, *33*(3), 243–265. https://doi.org/10.1029/2018GB005979

Kljun, N., Calanca, P., Rotach, M.W., & Schmid, H.P. (2015). A simple two-dimensional parameterisation for Flux Footprint Prediction (FFP). *Geoscientific Model Development*, *8*(11), 3695–3713. https://doi.org/10.5194/gmd-8-3695-2015

Kljun, N., Rotach, M.W., & Schmid, H.P. (2002). A Three-Dimensional Backward Lagrangian Footprint Model For A Wide Range Of Boundary-Layer Stratifications. *Boundary-Layer Meteorology*, *103*(2), 205–226. https://doi.org/10.1023/A:1014556300021

LiCor Biogeosciences. (2019, December 18). EddyPro® Software (Version 7.0.6) [Software]. LI-COR. https://www.licor.com/env/support/EddyPro/home.html

Liu, H., Zhang, Q., Katul, G.G., Cole, J.J., Chapin, F.S., & MacIntyre, S. (2016). Large $CO_2$ effluxes at night and during synoptic weather events significantly contribute to $CO_2$ emissions from a reservoir. *Environmental Research Letters*, *11*(6), 064001. https://doi.org/10.1088/1748-9326/11/6/064001

Lofton, M.E. (2022). melofton/FCR-phytos: Lofton et al. 20XX manuscript second revision (Version 3.0.0.). [Software]. Zenodo. https://doi.org/10.5281/zenodo.6483433

Loken, L. C., Crawford, J.T., Schramm, P.J., Stadler, P., Desai, A.R., & Stanley, E.H. (2019). Large Spatial and Temporal Variability of Carbon Dioxide and Methane in a Eutrophic Lake. *Journal of Geophysical Research: Biogeosciences*, *124*(7), 2248–2266. https://doi.org/10.1029/2019JG005186

MacIntyre, S., Jonsson, A., Jansson, M., Aberg, J., Turney, D.E., & Miller, S.D. (2010). Buoyancy flux, turbulence, and the gas transfer coefficient in a stratified lake. *Geophysical Research Letters*, *37*(24). https://doi.org/10.1029/2010GL044164

Mammarella, I., Nordbo, A., Rannik, Ü., Haapanala, S., Levula, J., Laakso, H., et. al. (2015). Carbon dioxide and energy fluxes over a small boreal lake in Southern Finland: $CO_2$ and Energy Fluxes Over Lake. *Journal of Geophysical Research: Biogeosciences*, *120*(7), 1296–1314. https://doi.org/10.1002/2014JG002873

Mauder, M., & Foken T. (2006). Impact of post-field data processing on eddy covariance flux estimates and energy balance closure. *Meteorologische Zietschrift, 15*, 597-609.

McClure, R.P., Hamre, K.D., Niederlehner, B.R., Munger, Z.W., Chen, S., Lofton, M.E., Schreiber, M.E., & Carey, C.C. (2018). Metalimnetic oxygen minima alter the vertical profiles of carbon dioxide and methane in a managed freshwater reservoir. *Science of The Total Environment*, *636*, 610–620. https://doi.org/10.1016/j.scitotenv.2018.04.255

McClure, R.P., Schreiber, M.E., Lofton, M.E., Chen, S., Krueger, K.M., & Carey, C.C. (2021). Ecosystem-Scale Oxygen Manipulations Alter Terminal Electron Acceptor Pathways in a Eutrophic Reservoir. *Ecosystems*, *24*(6), 1281–1298. https://doi.org/10.1007/s10021-020-00582-9

Moncrieff, J.B., Clement, R., Finnigan, J., Meyers, T. (2004). Averaging, Detrending, and Filtering of Eddy Covariance Time Series. In: Lee X., Massman W., Law B. (eds) *Handbook of Micrometeorology*. (Vol 29, pp. 7-31). Springer, Dordrecht. https://doi.org/10.1007/1-4020-2265-4_2

Moncrieff, J.B., Massheder, J.M.,de Bruin, H., Ebers, J., Friborg, T., Heusinkveld, B., et al. (1997). A system to measure surface fluxes of momentum, sensible heat, water vapor, and carbon dioxide. *Journal of Hydrology*, 188-189: 598-611. https://doi.org/10.1016/S0022-1694(96)03194-0

Ouyang, Z., Shao, C., Chu, H., Becker, R., Bridgeman, T., Stepien, C., John, R., & Chen, J. (2017). The Effect of Algal Blooms on Carbon Emissions in Western Lake Erie: An

Integration of Remote Sensing and Eddy Covariance Measurements. *Remote Sensing*, *9*(1), 44. https://doi.org/10.3390/rs9010044

Podgrajsek, E., Sahlée, E., Bastviken, D., Holst, J., Lindroth, A., Tranvik, L., & Rutgersson, A. (2014). Comparison of floating chamber and eddy covariance measurements of lake greenhouse gas fluxes. *Biogeosciences*, *11*(15), 4225–4233. https://doi.org/10.5194/bg-11-4225-2014

Podgrajsek, E., Sahlée, E., Bastviken, D., Natchimuthu, S., Kljun, N., Chmiel, H.E., Klemedtsson, L., & Rutgersson, A. (2016). Methane fluxes from a small boreal lake measured with the eddy covariance method: Methane fluxes from a small boreal lake. *Limnology and Oceanography*, *61*(S1), S41–S50. https://doi.org/10.1002/lno.10245

Prairie, Y.T., Alm, J., Beaulieu, J., Barros, N., Battin, T., Cole, J., et. al. (2018). Greenhouse Gas Emissions from Freshwater Reservoirs: What Does the Atmosphere See? *Ecosystems*, *21*(5), 1058–1071. https://doi.org/10.1007/s10021-017-0198-9

Read, J.S., Hamilton, D.P., Desai, A.R., Rose, K.C., MacIntyre, S., Lenters, J.D., et al. (2012). Lake-size dependency of wind shear and convection as controls on gas exchange: lake-size dependency of $u_*$ and $w_*$. *Geophysical Research Letters*, *39*(9). https://doi.org/10.1029/2012GL051886

Reed, D.E., Dugan, H.A., Flannery, A.L., & Desai, A.R. (2018). Carbon sink and source dynamics of a eutrophic deep lake using multiple flux observations over multiple years. *Limnology and Oceanography Letters*, *3*(3), 285–292. https://doi.org/10.1002/lol2.10075

Rosentreter, J.A., Borges, A.V., Deemer, B.R., Holgerson, M.A., Liu, S., Song, C., et al. (2021). Half of global methane emissions come from highly variable aquatic ecosystem sources. *Nature Geoscience*, *14*(4), 225–230. https://doi.org/10.1038/s41561-021-00715-2

Sanches, L.F., Guenet, B., Marinho, C.C., Barros, N., & de Assis Esteves, F. (2019). Global regulation of methane emission from natural lakes. *Scientific Reports*, *9*(1), 255. https://doi.org/10.1038/s41598-018-36519-5

Scholz, K., Ejarque, E., Hammerle, A., Kainz, M., Schelker, J., & Wohlfahrt, G. (2021). Atmospheric $CO_2$ Exchange of a Small Mountain Lake: Limitations of Eddy Covariance and Boundary Layer Modeling Methods in Complex Terrain. *Journal of Geophysical Research: Biogeosciences*, *126*(7). https://doi.org/10.1029/2021JG006286

Shao, C., Chen, J., Stepien, C.A., Chu, H., Ouyang, Z., Bridgeman, T.B., Czajkowski, K.P., Becker, R.H., & John, R. (2015). Diurnal to annual changes in latent, sensible heat, and $CO_2$ fluxes over a Laurentian Great Lake: A case study in Western Lake Erie. *Journal of Geophysical Research: Biogeosciences*, *120*(8), 1587–1604. https://doi.org/10.1002/2015JG003025

Sharma, S., Richardson, D.C., Woolway, R.I., Imrit, M.A., Bouffard, D., Blagrave, K., et. al. (2021). Loss of Ice Cover, Shifting Phenology, and More Extreme Events in Northern Hemisphere Lakes. *Journal of Geophysical Research: Biogeosciences*, *126*(10). https://doi.org/10.1029/2021JG006348

Sieczko, A. K., Duc, N.T., Schenk, J., Pajala, G., Rudberg, D., Sawakuchi, H.O., & Bastviken, D. (2020). Diel variability of methane emissions from lakes. *Proceedings of the National Academy of Sciences*, *117*(35), 21488–21494. https://doi.org/10.1073/pnas.2006024117

Smith, S.V., Renwick, W.H., Bartley, J.D., & Buddemeier, R.W. (2002). Distribution and significance of small, artificial water bodies across the United States landscape. *Science of The Total Environment*, *299*(1–3), 21–36. https://doi.org/10.1016/S0048-9697(02)00222-X

Sobek, S., Tranvik, L.J., & Cole, J.J. (2005). Temperature independence of carbon dioxide supersaturation in global lakes: Carbon dioxide supersaturation in global lakes. *Global Biogeochemical Cycles*, *19*(2),. https://doi.org/10.1029/2004GB002264

Soloviev, A., Donelan, M., Graber, H., Haus, B., & Schlüssel, P. (2007). An approach to estimation of near-surface turbulence and CO2 transfer velocity from remote sensing data. *Journal of Marine Systems*, *66*(1–4), 182–194. https://doi.org/10.1016/j.jmarsys.2006.03.023

Taoka, T., Iwata, H., Hirata, R., Takahashi, Y., Miyabara, Y., & Itoh, M. (2020). Environmental Controls of Diffusive and Ebullitive Methane Emissions at a Subdaily Time Scale in the Littoral Zone of a Midlatitude Shallow Lake. *Journal of Geophysical Research: Biogeosciences*, *125*(9). https://doi.org/10.1029/2020JG005753

Tranvik, L.J., Downing, J.A., Cotner, J.B., Loiselle, S.A., Striegl, R.G., Ballatore, T.J., et. al. (2009). Lakes and reservoirs as regulators of carbon cycling and climate. *Limnology and Oceanography*, *54*(6part2), 2298–2314. https://doi.org/10.4319/lo.2009.54.6_part_2.2298

USACE (United States Army Corps of Engineers). (2021). National inventory of Dams (NID). [accessed 2022 February 7]. https://nid.usace.army.mil/#/

Vachon, D., & Prairie, Y.T. (2013). The ecosystem size and shape dependence of gas transfer velocity versus wind speed relationships in lakes. *Canadian Journal of Fisheries and Aquatic Sciences*, *70*(12), 1757–1764. https://doi.org/10.1139/cjfas-2013-0241

Vesala, T., Eugster, W., & Ojala, A. (2012). Eddy Covariance Measurements over Lakes. In M. Aubinet, T. Vesala, & D. Papale (Eds.), *Eddy Covariance* (pp. 365–376). Springer Netherlands. https://doi.org/10.1007/978-94-007-2351-1_15

Vesala, T., Huotari, J., Rannik, Ü., Suni, T., Smolander, S., Sogachev, A., Launiainen, S., & Ojala, A. (2006). Eddy covariance measurements of carbon exchange and latent and sensible heat fluxes over a boreal lake for a full open-water period. *Journal of Geophysical Research*, *111*(D11), D11101. https://doi.org/10.1029/2005JD006365

Vickers, D., & Mahrt, L. (1997). Quality Control and Flux Sampling Problems for Tower and Aircraft Data. *Journal of Atmospheric and Oceanic Technology*, *14(*3), 512–526. https://doi.org/10.1175/1520-0426(1997)014<0512:QCAFSP>2.0.CO;2

Waldo, S., Beaulieu, J.J., Barnett, W., Balz, D. A., Vanni, M.J., Williamson, T., & Walker, J.T. (2021). Temporal trends in methane emissions from a small eutrophic reservoir: The key role of a spring burst. *Biogeosciences*, *18*(19), 5291–5311. https://doi.org/10.5194/bg-18-5291-2021

Watras, C.J., Morrison, K.A., Crawford, J.T., McDonald, C.P., Oliver, S.K., & Hanson, P.C. (2015). Diel cycles in the fluorescence of dissolved organic matter in dystrophic Wisconsin seepage lakes: Implications for carbon turnover: Diel CDOM fluorescence cycles. *Limnology and Oceanography*, *60*(2), 482–496. https://doi.org/10.1002/lno.10026

Webb, E.K., Pearman, G.I., & Leuning R. (1980). Correction of flux measurements for density effects due to heat and water vapour transfer. *Quarterly Journal of the Royal Meteorological Society*, *106*(447), 85-100. https://doi.org/10.1002/qj.49710644707

Wik, M., Thornton, B.F., Bastviken, D., Uhlbäck, J., & Crill, P.M. (2016). Biased sampling of methane release from northern lakes: A problem for extrapolation. *Geophysical Research Letters*, *43*(3), 1256–1262. https://doi.org/10.1002/2015GL066501

Wilczak, J.M., Oncley, S.P., Stage, S.A. (2001). Sonic anemometer tilt correction algorithms. *Boundary-Layer Meteorology*, 99, 127-150. https://doi.org/10.1023/A:1018966204465

Winslow, L. A., Read, J.S., Hanson, P.C., & Stanley, E.H. (2014). Lake shoreline in the contiguous United States: Quantity, distribution and sensitivity to observation resolution. *Freshwater Biology*, *59*(2), 213–223. https://doi.org/10.1111/fwb.12258

Winslow, L., Read, J., Woolway, R., Brentrup, J., Leach T., Zwart, J., Albers, S., & Collinge, C. (2016a, June 9). LakeAnalyzer: Lake Physics Tools. (Version 1.11.4.1). [Software]. R. Package. https://CRAN.R-project.org/package=rLakeAnalyzer

Winslow, L.A., Zwart, J.A., Batt, R.D., Dugan, H.A., Woolway, R.I., Corman, J.R., Hanson, P.C., & Read, J.S. (2016c). LakeMetabolizer: An R package for estimating lake metabolism from free-water oxygen using diverse statistical models. *Inland Waters*, *6*(4), 622–636. https://doi.org/10.1080/IW-6.4.883

Winslow, L., Zwart, J., Batt, R., Corman, J., Dugan, H., Hanson, P., et. al. (2016b, June 23). LakeMetabolizer: Tools for the analysis of ecosystem metabolism. (Version 1.5.0). [Software]. R Package. https://CRAN.R-project.org/pacakge=LakeMetabolizer

Woolway, R.I., Kraemer, B.M., Lenters, J.D., Merchant, C.J., O'Reilly, C.M., & Sharma, S. (2020). Global lake responses to climate change. *Nature Reviews Earth & Environment*, *1*(8), 388–403. https://doi.org/10.1038/s43017-020-0067-5

Wutzler, T., Lucas-Moffat, A., Migliavacca, M., Knauer, J., Sickel, K., Šigut, L., Menzer, O., & Reichstein, M. (2018). Basic and extensible post-processing of eddy covariance flux data with REddyProc. *Biogeosciences*, *15*(16), 5015–5030. https://doi.org/10.5194/bg-15-5015-2018

Wutzler, T., Reichstein, M., Lucas-Moffat, A.M., Menzer, O., Migliavacca, M., & Sickel, K. (2021, December 01). REddyProc: Post Processing of (Half-) Hourly Eddy-Covariance Measurements. (Version 1.3.1). [Software]. R. Package. https://CRAN.R-project.org/package=REddyProc

Supporting Information for

# Eddy covariance data reveal that a small freshwater reservoir emits a substantial amount of carbon dioxide and methane

Alexandria G. Hounshell[1, †], Brenda M. D'Acunha[2], Adrienne Breef-Pilz[1], Mark S. Johnson[2,3], R. Quinn Thomas[1,4], Cayelan C. Carey[1]

[1] Department of Biological Sciences, Virginia Tech, Blacksburg, VA, USA, [2] Department of Earth, Ocean, and Atmospheric Sciences, University of British Columbia, Vancouver, BC, Canada, [3] Institute for Resources, Environment and Sustainability, University of British Columbia, Vancouver, BC, Canada, [4] Department of Forest Resources and Environmental Conservation, Virginia Tech, Blacksburg, VA, USA

Corresponding author: Alexandria G. Hounshell (alexgh@vt.edu)

† Current affiliation: National Centers for Coastal Ocean Science, National Oceanographic and Atmospheric Administration, Beaufort, NC, 28516, alexandria.hounshell@noaa.gov

## Contents of this file

Figures S1 to S12
Tables S1 to S9

## Introduction

The supplementary information additional figures (Figures S1-S12) and tables (Tables S1-S9) used as supporting information in the associated manuscript.

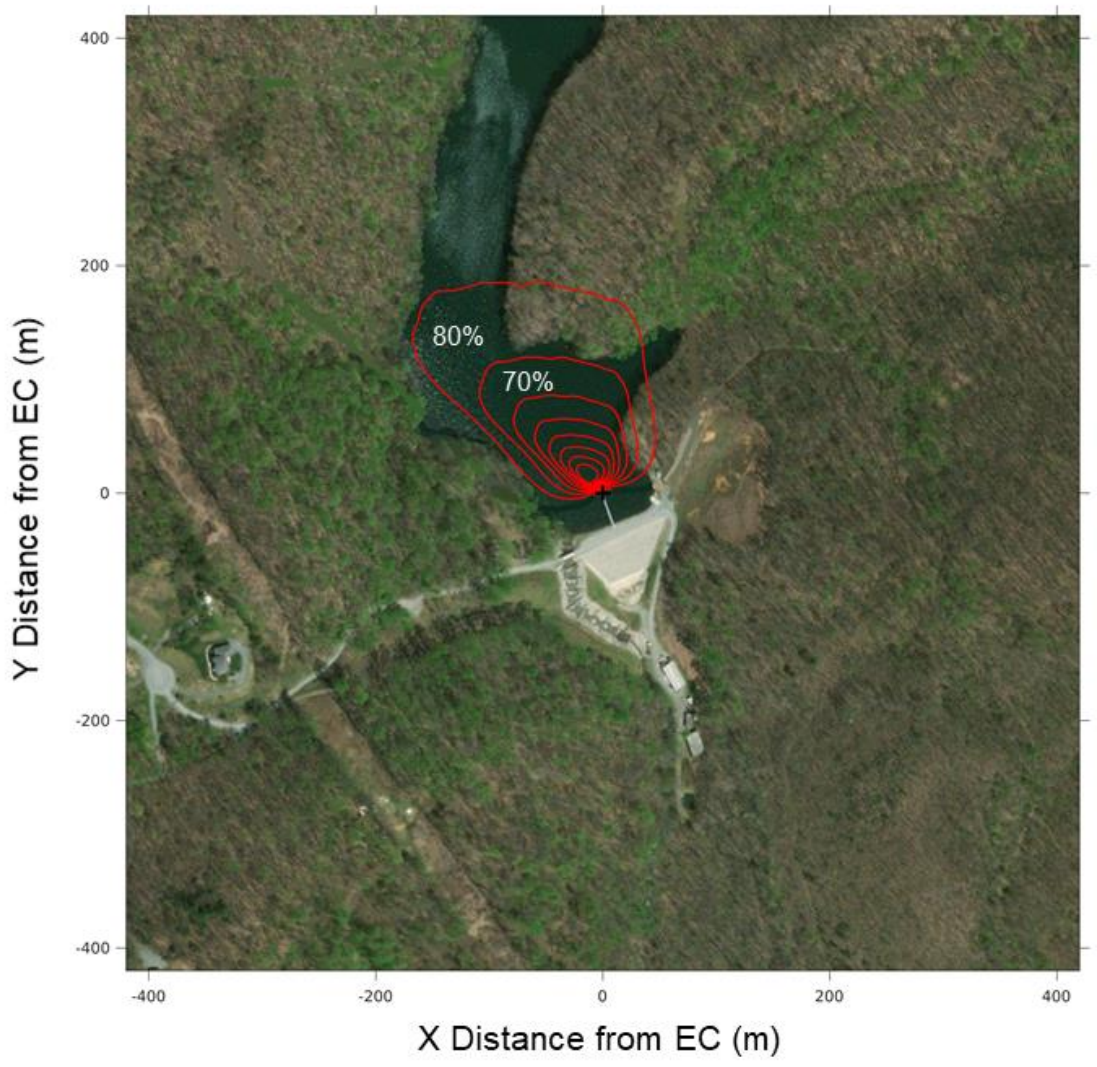


**Figure S1.** Cumulative footprint for the two years of eddy covariance (EC) fluxes measured from Falling Creek Reservoir following methods in Kljun et al. (2015). The 10-80% isolines are plotted as red circles around the EC system (denoted as the black plus-sign).

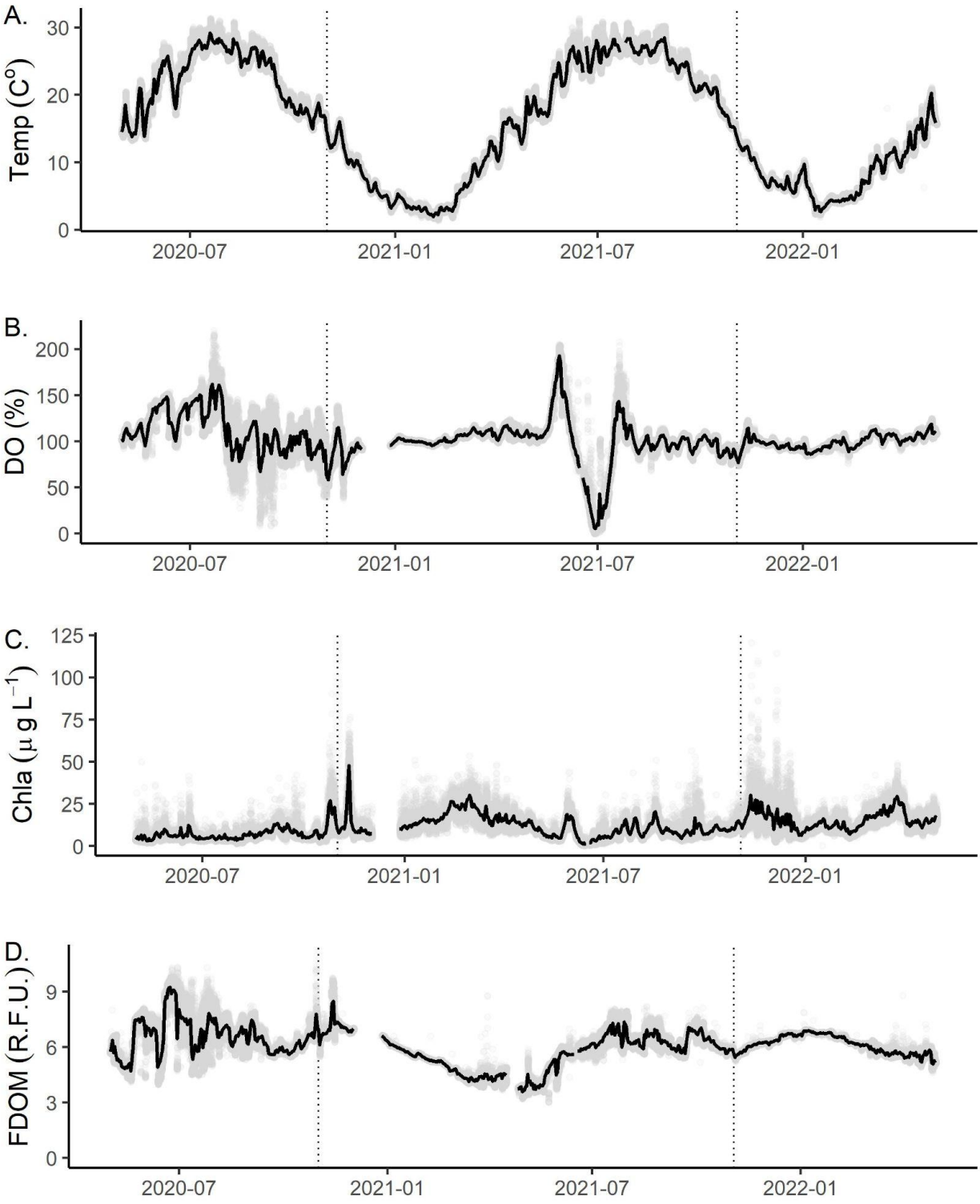


**Figure S2.** Environmental variables measured during the study period, including A. Surface Water Temperature (Temp, °C) measured at 0.1 m below the surface; B. Dissolved oxygen (DO, percent saturation, %) measured at 1.6 m; C. Chlorophyll-*a* (Chl-a, µg $L^{-1}$)

measured at 1.6 m; and D. fluorescent dissolved organic matter (fDOM, Relative Fluorescence Units, RFU) measured at 1.6 m. Solid black lines represent the daily mean while the light grey points represent individual measurements made every 15 minutes for inflow and every 10 minutes for all other variables. The dashed vertical black line indicates reservoir fall turnover for both years.

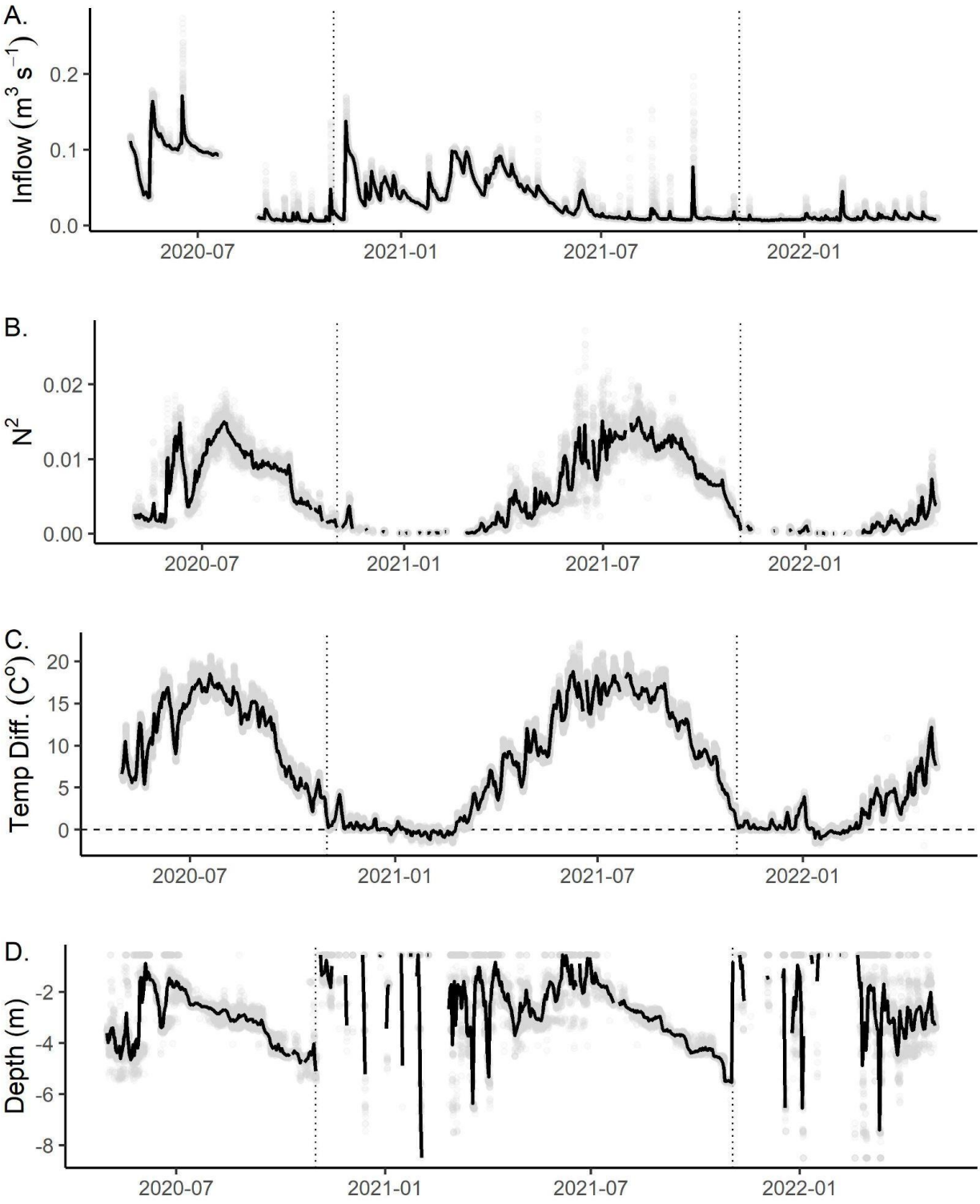


**Figure S3.** Environmental variables measured during the study period, including A. Inflow ($m^3$ $s^{-1}$) measured at the primary inflow to Falling Creek Reservoir; B. Buoyancy frequency ($N^2$) calculated from thermal profiles at the deepest point in the reservoir; C.

The temperature difference (Temp Diff., °C) measured from the surface (0.1 m) and bottom (9 m) at the deepest point of the reservoir; and D. Thermocline depth (Depth, m) calculated from thermal profiles deployed at the deepest point of the reservoir. Solid black lines represent the daily mean while the light grey points represent individual measurements made every 15 minutes for inflow and every 10 minutes for all other variables. The dashed vertical black line indicates reservoir fall turnover for each year.

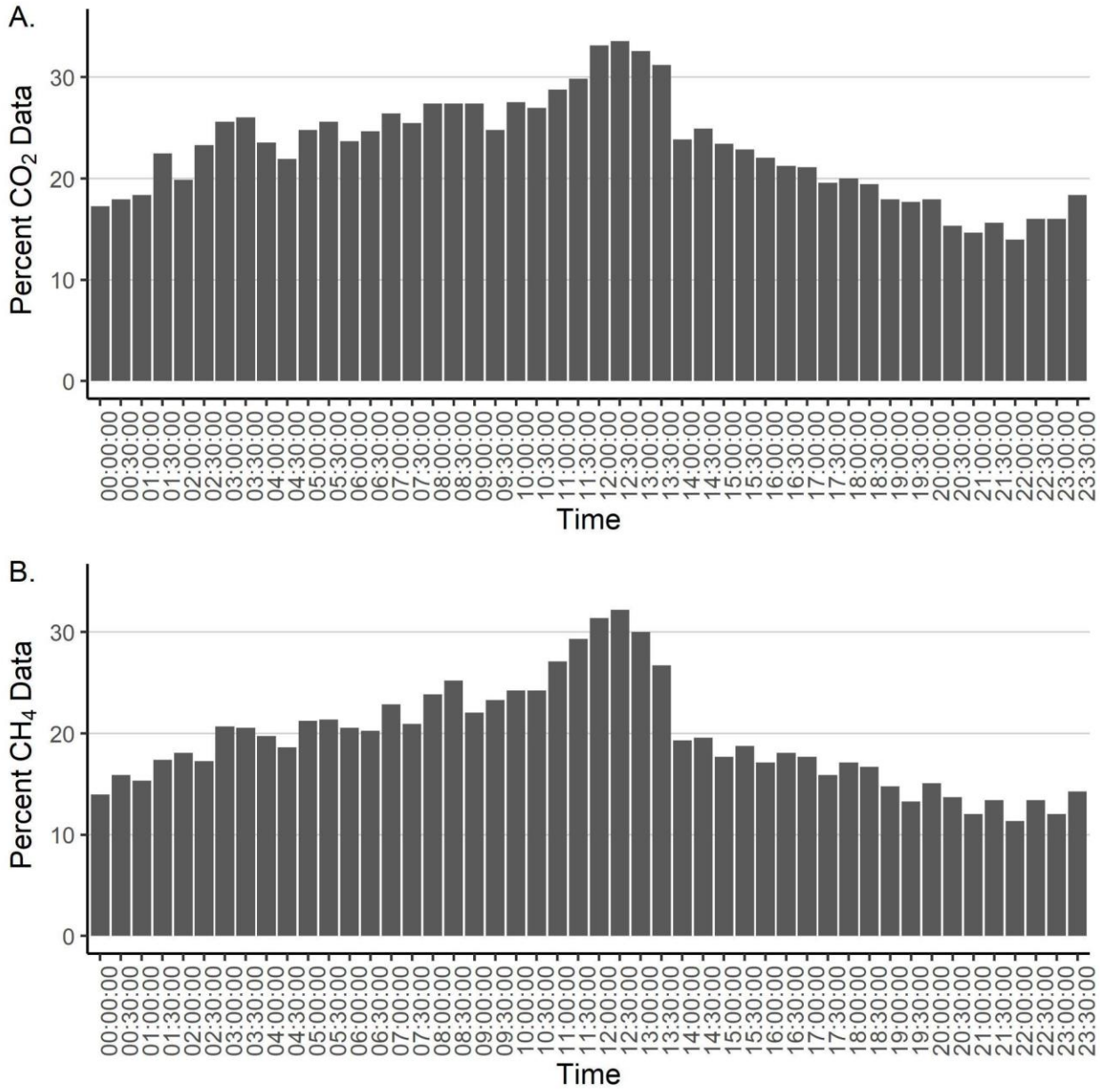


**Figure S4.** Barplot of average percent of data availability for A. carbon dioxide ($CO_2$) and B. methane ($CH_4$) fluxes distributed throughout the day (half-hourly from 0:00 to 23:30).

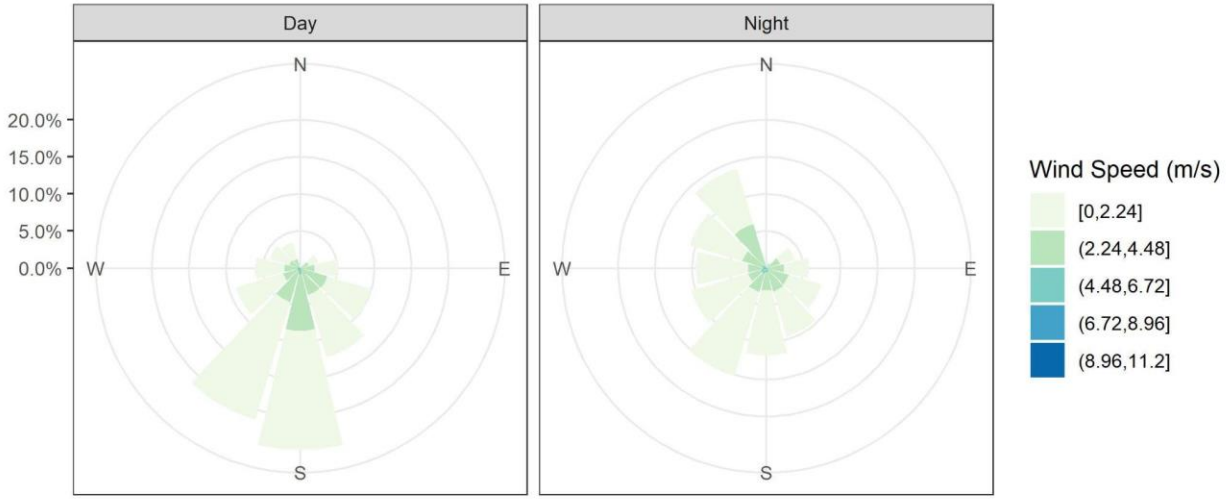


**Figure S5**. Windrose of all measured windspeed and direction during the study period separated by A. Day (shortwave radiation in > 0 W $m^2$) and B. Night (shortwave radiation in < 0 W $m^2$) collected from the meteorological stations deployed at the dam.

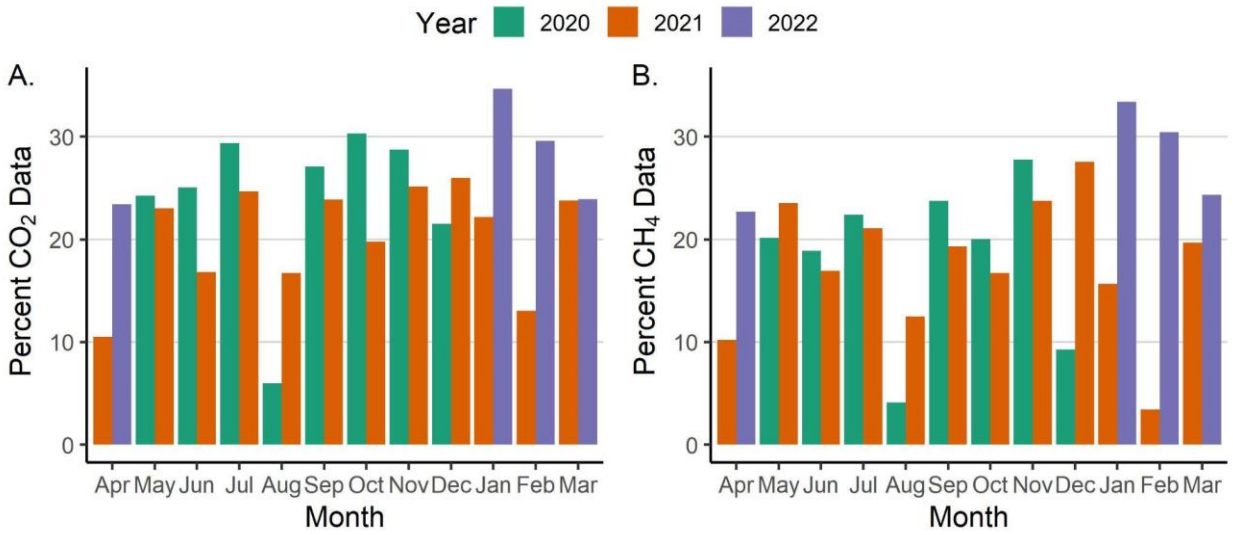


**Figure S6.** Barplot of average percent of data availability for A. carbon dioxide ($CO_2$) and B. methane ($CH_4$) fluxes distributed throughout each month and year of the study period.

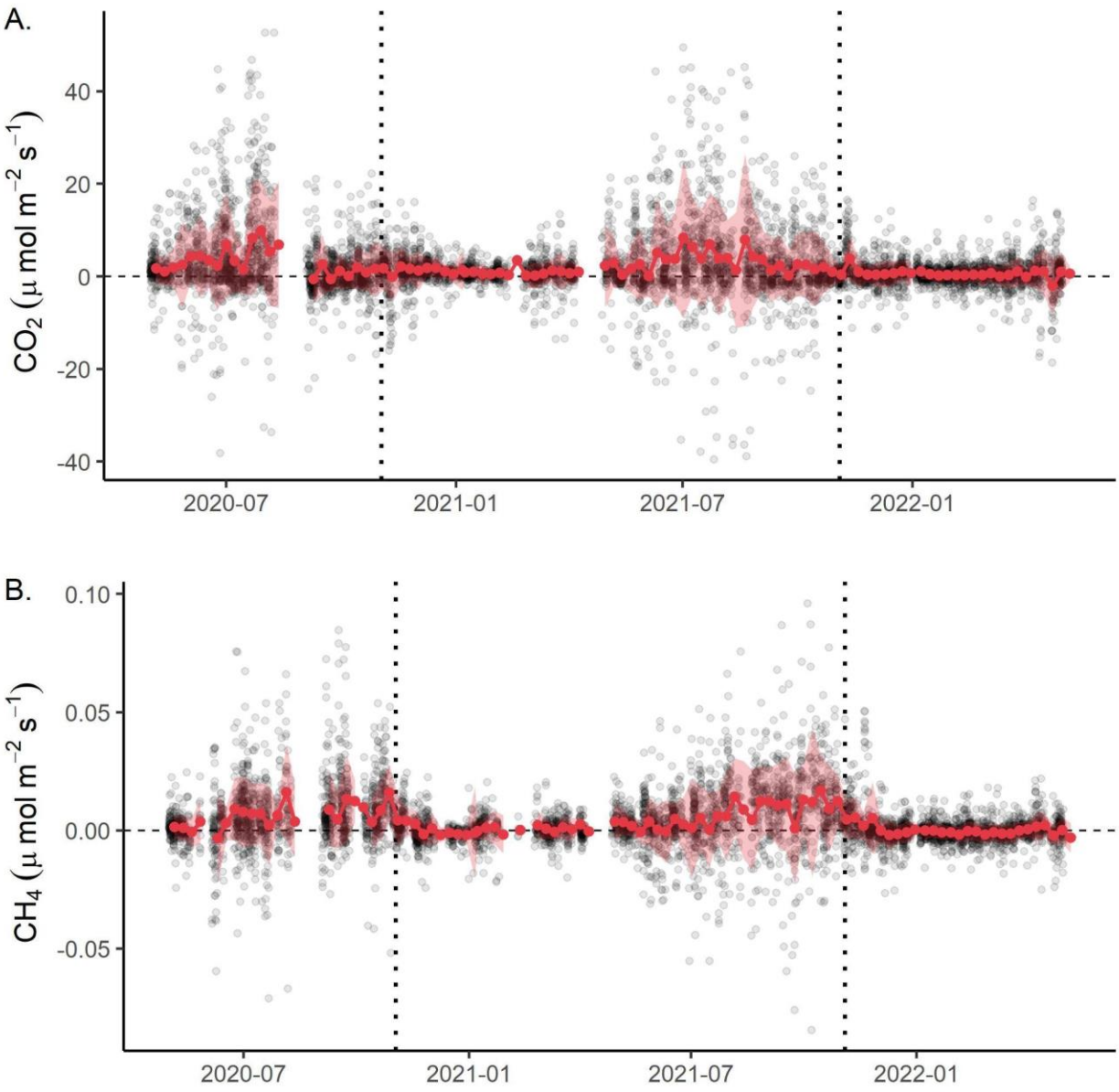


**Figure S7.** A. Mean weekly carbon dioxide fluxes ($CO_2$, μmol $m^{-2}$ $s^{-1}$) and B. mean weekly methane fluxes ($CH_4$, μmol $m^{-2}$ $s^{-1}$) aggregated from measured eddy covariance data from 1 May 2020 to 30 April 2021 in Falling Creek Reservoir plotted as a red line with dots. The red shaded area corresponds to the standard deviation (±1 S.D.) of aggregated fluxes for both measured and gap-filled values. Black dots represent measured half-hourly fluxes. The vertical dashed line corresponds to reservoir fall turnover for each year.

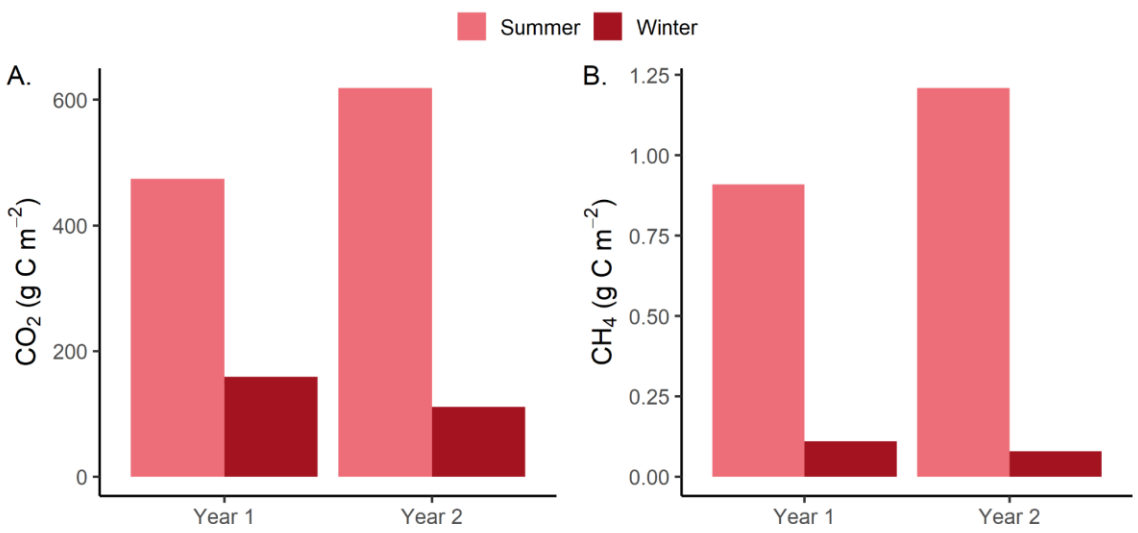


**Figure S8.** Comparison of cumulative fluxes from summer (May - October) and Winter (November - April) for year 1 (2020-2021) and year 2 (2021-2022) for A. carbon dioxide ($CO_2$, g C $m^{-2}$) and B. methane ($CH_4$, g C $m^{-2}$).

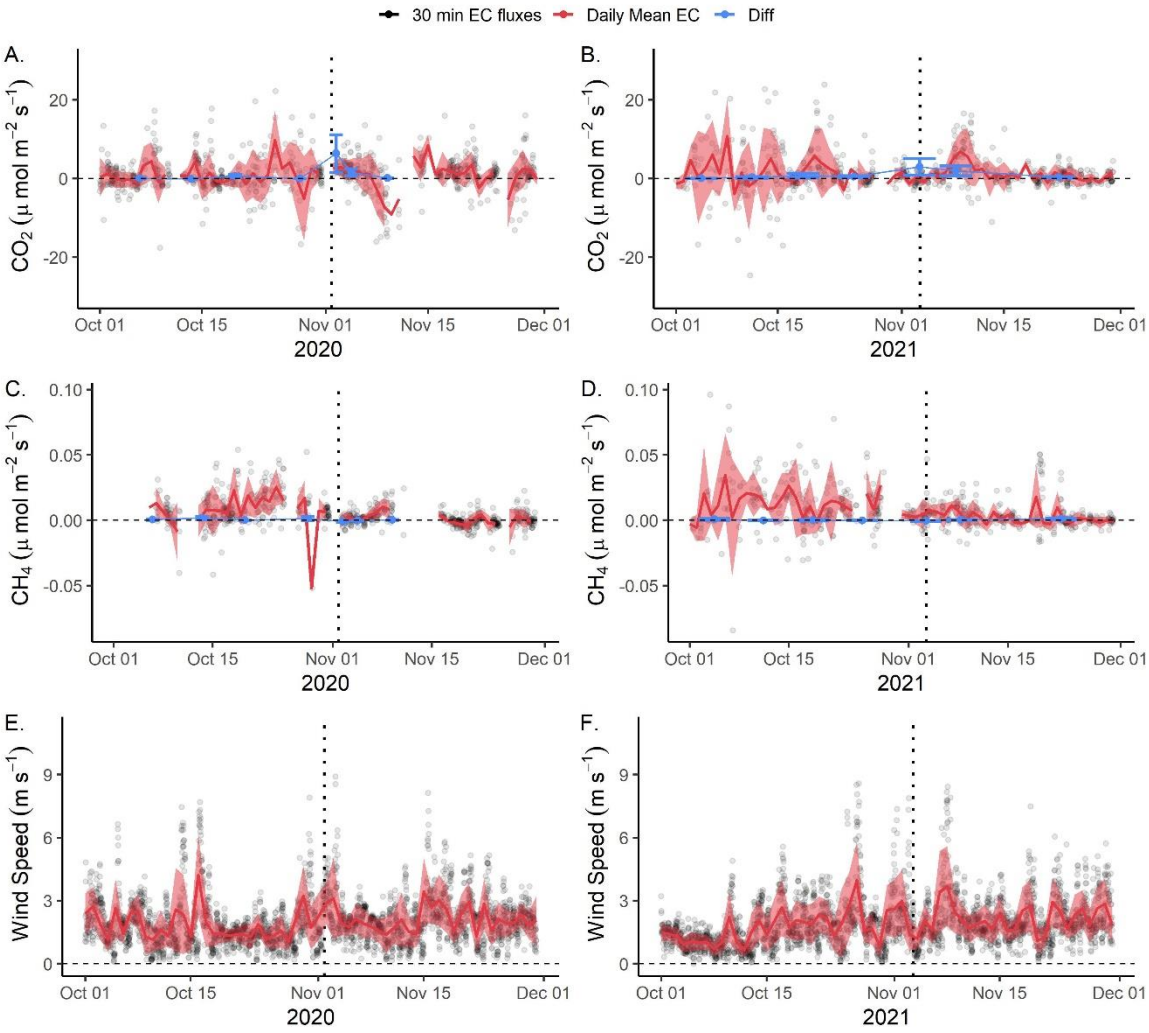


**Figure S9.** Mean daily A., B. Carbon dioxide ($CO_2$, μmol $m^{-2}$ $s^{-1}$) and C., D. Mean daily methane fluxes ($CH_4$ μmol $m^{-2}$ $s^{-1}$) for 2020 and 2021, respectively, around reservoir fall turnover (01 November 2021 and 03 November 2022, respectively). Mean daily wind is also plotted for E. 2020 and F. 2021. Grey dots represent measured half-hourly fluxes from the EC system ($CO_2$, $CH_4$) and the meteorological station deployed at the dam of Falling Creek Reservoir (Wind speed). The dark red line represents daily mean fluxes or wind speed. The shaded red area represents ±1 standard deviation of the daily 30-minute fluxes or wind speed. The vertical dotted line indicates reservoir fall turnover.

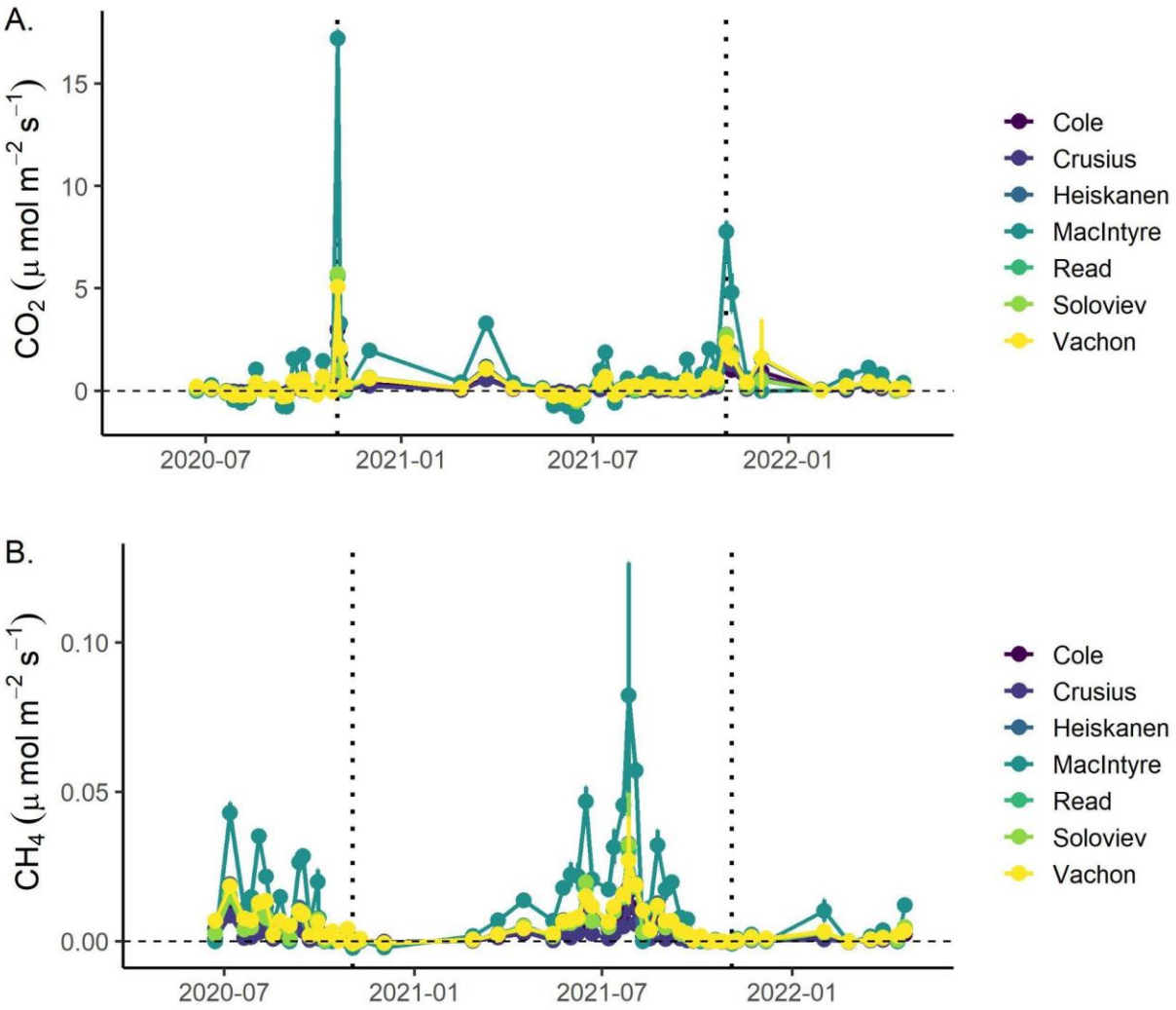


**Figure S10.** Discrete diffusive fluxes calculated for A. carbon dioxide ($CO_2$, µmol $m^{-2}$ $s^{-1}$) and B. methane ($CH_4$, µmol $m^{-2}$ $s^{-1}$) during the study period (1 May 2020 to 30 April 2022) using multiple gas transfer coefficient models (k; Winslow et al. 2016; Cole and Caraco, 1998; Crusius and Wannikof, 2003; Vachon and Prairie, 2013; MacIntyre et al. 2010; Heiskanen et al. 2014; Read et al. 2012; Soloviev et al. 2007). Points represent the mean of two replicates calculated for each k method and the error bars are the standard deviation (±1 S.D.). The dashed horizontal line indicates zero fluxes and the dotted vertical line corresponds to reservoir fall turnover on 1 November 2020 and 3 November 2021, respectively.

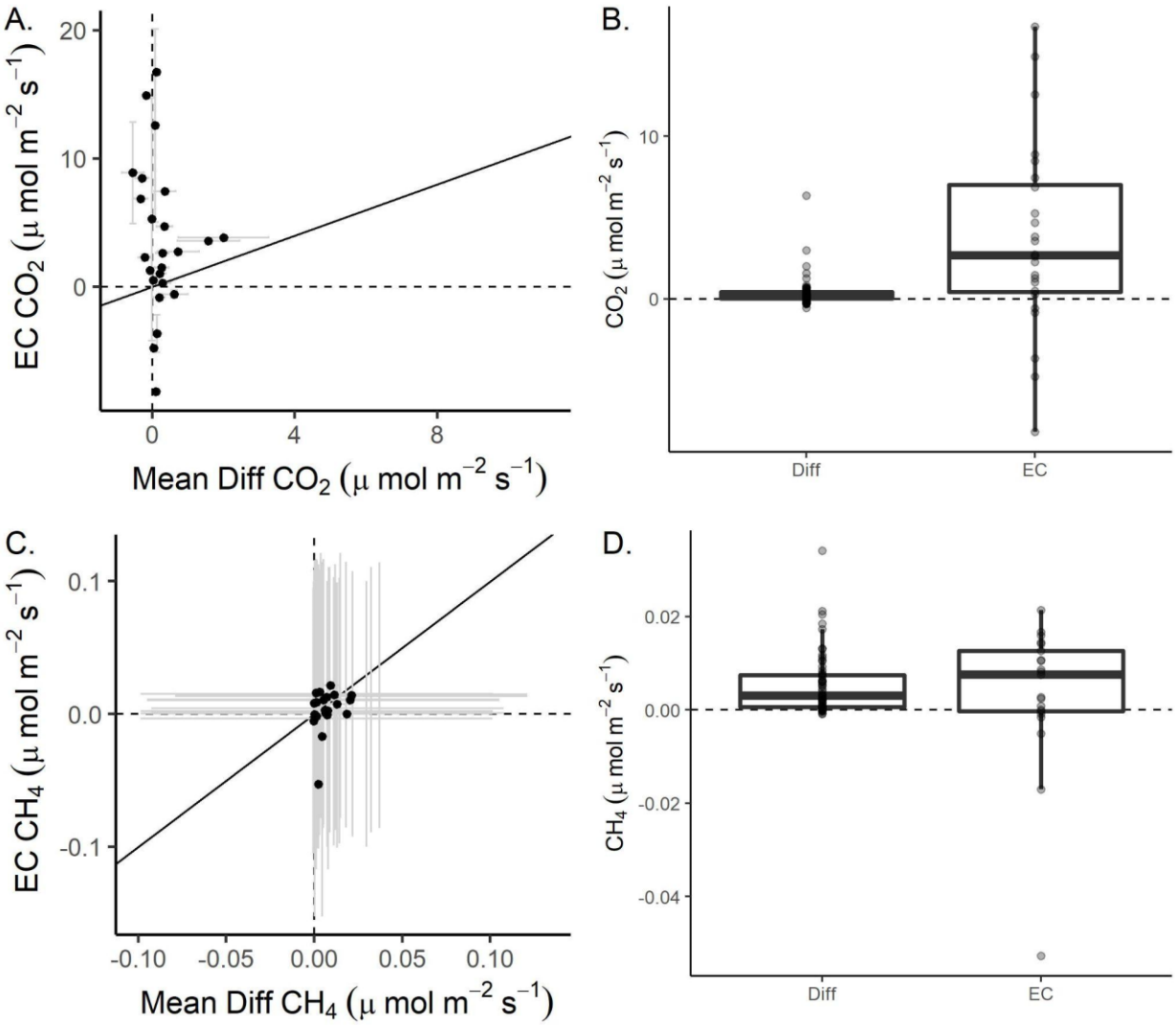


**Figure S11.** Instantaneous mean diffusive fluxes compared to mean hourly fluxes obtained using the eddy covariance (EC) system for A. carbon dioxide ($CO_2$, μmol $m^{-2}$ $s^{-1}$; n = 24 observations) and C. methane ($CH_4$, μmol $m^{-2}$ $s^{-1}$; n = 21 observations). Standard deviation is plotted as grey bars for both mean diffusive fluxes estimated for two replicates using all k methods (see main manuscript text) and for mean hourly fluxes obtained using the EC. Results are also compared as boxplots for B. $CO_2$ and D. $CH_4$ where the mean instantaneous fluxes are plotted as the grey points; the box represents the 25th and 75th percentiles; the median is represented as the bolded line; and the whiskers represent the minimum and maximum values (1.5x interquartile range). Dashed vertical and horizontal lines correspond to zero fluxes; the one-to-one line is plotted as a solid black line.

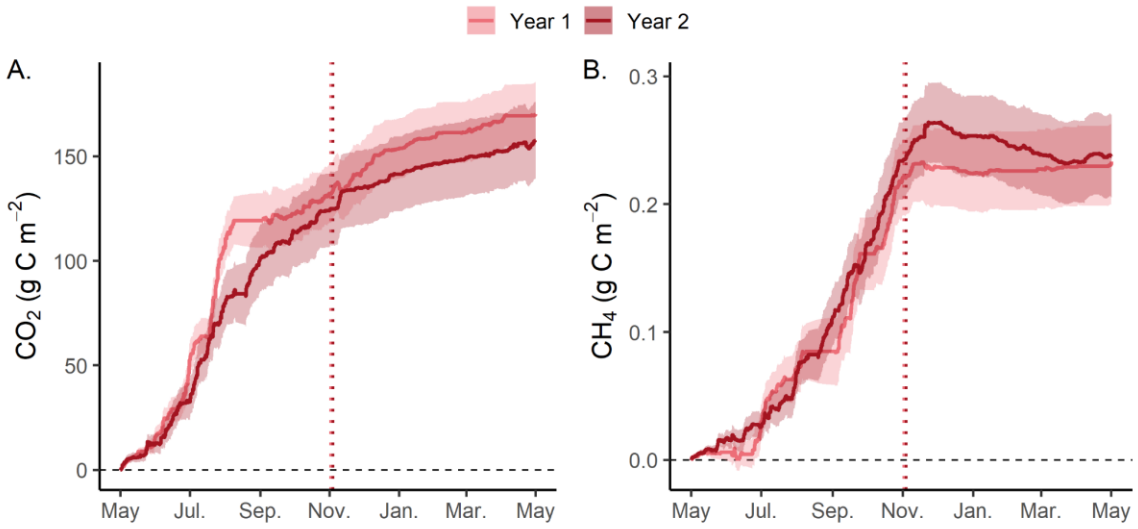


**Figure S12.** Annual cumulative fluxes for A. carbon dioxide ($CO_2$, g C $m^{-2}$) and B. methane ($CH_4$, g C $m^{-2}$) using measured eddy covariance fluxes from Falling Creek Reservoir for Year 1 (May 2020-April 2021; pink) and Year 2 (May 2021-April 2022; dark red). Shaded areas correspond to the aggregated standard deviation (±1 S.D.) of measurements. The horizontal dashed line corresponds to zero and the vertical dotted line indicates reservoir fall turnover for both years. Note: these cumulative fluxes only represent 22 and 24% of $CO_2$ fluxes and 16 and 23% of $CH_4$ fluxes measured directly using the EC system in year 1 and year 2, respectively. When upscaling to the full year, this would lead to 774 and 657 g $CO_2$ $m^{-2}$ for year 1 and year 2 and 1.45 and 1.03 g $CH_4$ $m^{-2}$, respectively.

| | Start Date | End Date |
|---|---|---|
| Intermittent Ice on | 10 January 2021 | 10 February 2021 |
| Continuous Ice on | 16 January 2022 | 10 February 2022 |

**Table S1.** Start and end dates used to define intermittent ice-on and continuous ice-on periods during the winter for 2020-2021 and winter 2021-2022 in Falling Creek Reservoir (Carey and Breef-Pilz, 2022).

**Hourly**

| | DO % Sat. | Chl-a (µg $L^{-1}$) | fDOM (RFU) | Inflow ($m^3$ $s^{-1}$) | Temp Diff. | $N^2$ | Thermo Depth (m) |
|---|---|---|---|---|---|---|---|
| **Surface Temp. (ºC)** | 0.09 | -0.50 | 0.39 | 0.04 | 0.94 | 0.90 | -0.18 |
| **DO % Sat.** | | 0.05 | 0.10 | 0.41 | 0.19 | 0.05 | -0.15 |
| **Chl-a (µg $L^{-1}$)** | | | -0.19 | -0.21 | -0.46 | -0.42 | 0.05 |
| **fDOM (RFU)** | | | | 0.19 | 0.32 | 0.32 | -0.11 |
| **Inflow ($m^3$ $s^{-1}$)** | | | | | 0.17 | 0.01 | -0.23 |
| **Temp Diff.** | | | | | | 0.89 | -0.34 |
| **$N^2$** | | | | | | | -0.29 |

**Daily**

| | | | | | | | |
|---|---|---|---|---|---|---|---|
| **Surface Temp. (ºC)** | 0.04 | -0.54 | 0.30 | 0.02 | 0.94 | 0.91 | -0.01 |
| **DO % Sat.** | | 0.10 | 0.01 | 0.39 | 0.12 | 0.00 | -0.05 |
| **Chl-a (µg $L^{-1}$)** | | | -0.18 | -0.16 | -0.53 | -0.49 | -0.02 |
| **fDOM (RFU)** | | | | 0.13 | 0.23 | 0.28 | -0.05 |
| **Inflow ($m^3$ $s^{-1}$)** | | | | | 0.14 | -0.03 | -0.18 |
| **Temp Diff.** | | | | | | 0.92 | -0.17 |
| **$N^2$** | | | | | | | -0.15 |

**Weekly**

| | | | | | | | |
|---|---|---|---|---|---|---|---|
| **Surface Temp. (ºC)** | 0.10 | -0.52 | 0.18 | 0.06 | 0.95 | 0.93 | 0.16 |
| **DO % Sat.** | | 0.07 | -0.07 | 0.39 | 0.17 | 0.06 | -0.01 |
| **Chl-a (µg $L^{-1}$)** | | | -0.25 | -0.19 | -0.52 | -0.50 | -0.07 |
| **fDOM (RFU)** | | | | 0.11 | 0.11 | 0.21 | -0.09 |
| **Inflow ($m^3$ $s^{-1}$)** | | | | | 0.14 | 0.00 | -0.17 |
| **Temp Diff.** | | | | | | 0.95 | 0.01 |
| **$N^2$** | | | | | | | -0.01 |

| | Monthly | | | | | | |
|---|---|---|---|---|---|---|---|
| | **DO % Sat.** | **Chl-a ($\mu g\ L^{-1}$)** | **fDOM (RFU)** | **Inflow ($m^3\ s^{-1}$)** | **Temp Diff.** | **$N^2$** | **Thermo Depth (m)** |
| **Surface Temp. (ºC)** | 0.16 | -0.68 | 0.23 | 0.03 | 0.96 | 0.95 | 0.03 |
| **DO % Sat.** | | -0.15 | -0.14 | 0.65 | 0.23 | 0.11 | 0.00 |
| **Chl-a ($\mu g\ L^{-1}$)** | | | -0.45 | -0.18 | -0.68 | -0.64 | 0.05 |
| **fDOM (RFU)** | | | | -0.03 | 0.16 | 0.30 | -0.04 |
| **Inflow ($m^3\ s^{-1}$)** | | | | | 0.13 | 0.01 | -0.27 |
| **Temp Diff.** | | | | | | 0.96 | -0.12 |
| **$N^2$** | | | | | | | -0.11 |

**Table S2.** Correlations (Pearson's rho) among environmental parameters identified for the ARIMA analyses, including surface temperature (surface temp., °C), percent dissolved oxygen saturation (DO % Sat.), chlorophyll-*a* (Chl-a, $\mu g\ L^{-1}$), fluorescent dissolved organic matter (fDOM, relative fluorescence units, RFU), inflow ($m^3\ s^{-1}$), temperature difference (Temp Diff.) between the surface (0.1 m) and bottom (9 m), and buoyancy frequency ($N^2$). Highlighted boxes indicate environmental variables which were removed due to collinearity (rho>|0.70|).

| | Percent available $CO_2$ fluxes (%) | Percent available $CH_4$ fluxes (%) |
|---|---|---|
| Raw data available | 84 | 73 |
| Removing fluxes from behind the dam (<80° and >250°) | 59 | 52 |
| QA/QC* of fluxes, LE**, and H*** | 39 | 33 |
| Removing fluxes outside of reservoir footprint | 29 | 25 |
| Removing fluxes with low u* | 23 | 19 |

* QA/QC = Quality assurance/quality control
** Latent energy flux
*** Sensible heat flux

**Table S3.** Percent of measured carbon dioxide ($CO_2$) and methane ($CH_4$) fluxes retained for analysis following data post-processing and various steps of data post-processing. See main manuscript for description of each post-processing step; all code is available in (Carey et al. 2022a).

| | | Minimum (µmol $m^{-2}$ $s^{-1}$) | Maximum (µmol $m^{-2}$ $s^{-1}$) | Median (µmol $m^{-2}$ $s^{-1}$) | Mean (µmol $m^{-2}$ $s^{-1}$) | Standard Deviation (µmol $m^{-2}$ $s^{-1}$) | Coefficient of Variation (%) |
|---|---|---|---|---|---|---|---|
| **$CH_4$** | Measured EC | -0.084 | 0.096 | 0.001 | 0.003 | 0.011 | 350.571 |
| | Diffusive (Mean) | -0.0059 | 0.0928 | 0.0020 | 0.0048 | 0.0074 | 154.62 |
| **$CO_2$** | Measured EC | -39.46 | 52.67 | 0.79 | 1.86 | 6.21 | 334.21 |
| | Diffusive (Mean) | -1.24 | 17.50 | 0.11 | 0.38 | 1.22 | 325.66 |

**Table S4.** Minimum, maximum, median, mean, standard deviation, and coefficient of variation for measured methane ($CH_4$) and carbon dioxide ($CO_2$) fluxes for the study period (1 May 2020 to 30 April 2022) obtained from the eddy covariance (EC) system and mean diffusive fluxes. Mean diffusive fluxes represent all diffusive methods.

| | 25th Percentile | Median | 75th Percentile | *p*-value |
|---|---|---|---|---|
| | **$CO_2$ (µmol $m^{-2}$ $s^{-1}$)** | | | |
| Day | -0.44 | 1.05 | 3.91 | |
| Night | -0.60 | 1.03 | 3.48 | 0.093 |
| Dawn | -0.07 | 1.34 | 4.37 | |
| Dusk | -0.66 | -0.03 | 0.65 | <0.001 |
| | **$CH_4$ (µmol $m^{-2}$ $s^{-1}$)** | | | |
| Day | -0.0017 | 0.0013 | 0.0079 | |
| Night | -0.0016 | 0.0011 | 0.0066 | 0.162 |
| Dawn | -0.0027 | 0.0002 | 0.0052 | |
| Dusk | -0.0008 | 0.0014 | 0.0062 | 0.357 |
| | **Wind (m $s^{-1}$)** | | | |
| Day | 0.92 | 1.27 | 1.73 | |
| Night | 0.76 | 1.03 | 1.44 | <0.001 |
| Dawn | 0.95 | 1.24 | 1.64 | |
| Dusk | 0.87 | 1.23 | 1.67 | 0.003 |

**Table S5.** Diel (day/night) and dawn/dusk comparisons for measured eddy covariance (EC) fluxes for carbon dioxide ($CO_2$, µmol $m^{-2}$ $s^{-1}$) and methane ($CH_4$, µmol $m^{-2}$ $s^{-1}$) along with wind (m $s^{-1}$). Day corresponds to measurements collected from 1100 to 1300 while night corresponds to 2300 to 0100 throughout the time period. Dawn corresponds to measurements collected from 0500 to 0700 and dusk corresponds to 1700 to 1900. Statistically significant differences ($p < 0.05$) based on paired Wilcoxon sign-rank tests are highlighted in grey.

| | Year 1 | Year 2 | Total Study Period |
|---|---|---|---|
| Mean Temp. (°C) | 13.8 | 14.4 | 14.1 |
| Min. Temp. (°C) | -9.93 | -11.5 | |
| Max. Temp. (°C) | 35.1 | 35.0 | |
| Mean Wind Speed ($m\ s^{-1}$) | 2.00 | 1.97 | 1.99 |
| Max. Wind Speed ($m\ s^{-1}$) | 9.28 | 11.2 | |
| Dominant Wind Direction (°) | 191 | 199 | 198 |
| Total Rainfall (mm) | 1438 | 790 | 2228 |

**Table S6.** Various climatological variables calculated for Falling Creek Reservoir (FCR) for Year 1 (01 May 2020-30 April 2021), Year 2 (01 May 2021-30 April 2022), and the full study period calculated from the meteorological station deployed at the dam.

| | Year 1 | Year 2 | Total Study Period |
|---|---|---|---|
| Mean Surface Temp. (°C) | 15.2 | 15.9 | 15.6 |
| Min. Surface Temp. (°C) | 1.23 | 1.88 | |
| Max. Surface Temp. (°C) | 31.4 | 31.3 | |
| Mean Chl-a (µg $L^{-1}$) | 11.5 | 12.3 | 11.9 |
| Min. Chl-a (µg $L^{-1}$) | 1.34 | 0.25 | |
| Max Chla (µg $L^{-1}$) | 90.3 | 121 | |
| Mean fDOM (RFU) | 6.09 | 6.04 | 6.1 |
| Min. fDOM (RFU) | 3.19 | 3.01 | |
| Max. fDOM (RFU) | 10.4 | 8.79 | |
| Mean % DO | 107 | 97.8 | 102 |
| Min. % DO | 8.12 | 0 | |
| Max. % DO | 220 | 208 | |
| Mean Inflow ($m^3$ $s^{-1}$) | 0.056 | 0.013 | 0.034 |
| Min. Inflow ($m^3$ $s^{-1}$) | 0.005 | 0.006 | |
| Max. Inflow ($m^3$ $s^{-1}$) | 0.27 | 0.20 | |

**Table S7.** Mean, minimum, and maximum calculated for key environmental variables from Falling Creek Reservoir during year 1 (May 2020 - April 2021) and year 2 (May 2021 - April 2022) including: Surface temperature, Chlorophyll-a (Chl-a), fluorescent dissolved organic matter (fDOM, RFU), percent dissolved oxygen (% DO), and inflow.

| GHG | Order | AR(1) | MA(1) | MA(2) | Temp. Surf. (ºC) | % DO Sat. | Chl-a (µg $L^{-1}$) | fDOM (RFU) | Flow ($m^3$ $s^{-1}$) | Thermo. (m) | AICc | RMSE |
|---|---|---|---|---|---|---|---|---|---|---|---|---|
| | | | | | | Daily | | | | | | |
| $CO_2$ | (1,0,0) | 0.11 | | | 0.18 | | -0.17 | 0.07 | 0.08 | -0.09 | 1281.69 | 0.97 |
| S.E. | | 0.05 | | | 0.07 | | 0.06 | 0.05 | 0.05 | 0.05 | | |
| $CO_2$ | (1,0,0) | 0.10 | | | 0.20 | -0.07 | -0.14 | 0.07 | 0.12 | -0.09 | 1281.79 | 0.97 |
| S.E. | | 0.05 | | | 0.07 | 0.05 | 0.06 | 0.05 | 0.06 | 0.05 | | |
| $CO_2$ | (0,0,2) | | 0.11 | 0.05 | 0.20 | | -0.17 | | 0.08 | -0.09 | 1282.98 | 0.97 |
| S.E. | | | 0.05 | 0.05 | 0.07 | | 0.06 | | 0.05 | 0.05 | | |
| $CO_2$ | (0,0,2) | | 0.10 | 0.04 | 0.22 | -0.07 | -0.15 | | 0.11 | -0.09 | 1283.35 | 0.97 |
| S.E. | | | 0.05 | 0.05 | 0.07 | 0.05 | 0.06 | | 0.06 | 0.05 | | |
| $CH_4$ | (0,0,0) | | | | 0.27 | | | 0.12 | | 0.25 | 1213.36 | 1.02 |
| S.E. | | | | | 0.05 | | | 0.05 | | 0.05 | | |
| $CH_4$ | (0,0,0) | | | | 0.28 | -0.04 | | 0.12 | | 0.25 | 1214.53 | 1.02 |
| S.E. | | | | | 0.05 | 0.04 | | 0.05 | | 0.05 | | |
| $CH_4$ | (0,0,0) | | | | 0.28 | | 0.02 | 0.12 | | 0.25 | 1215.30 | 1.02 |
| S.E. | | | | | 0.07 | | 0.06 | 0.05 | | 0.05 | | |

| GHG | Order | AR(1) | MA(1) | MA(2) | Temp. Surf. (ºC) | % DO Sat. | Chl-a (µg $L^{-1}$) | fDOM (RFU) | Flow ($m^3$ $s^{-1}$) | Thermo. (m) | AICc | RMSE |
|---|---|---|---|---|---|---|---|---|---|---|---|---|
| | | | | | | Weekly | | | | | | |
| $CO_2$ | (0,0,0) | | | | 0.64 | -0.16 | | 0.13 | 0.20 | -0.19 | 183.00 | 0.63 |
| S.E. | | | | | 0.07 | 0.07 | | 0.07 | 0.08 | 0.07 | | |
| $CO_2$ | (0,0,0) | | | | 0.67 | -0.17 | | | 0.19 | -0.20 | 184.05 | 0.64 |
| S.E. | | | | | 0.07 | 0.07 | | | 0.08 | 0.07 | | |
| $CH_4$ | (0,1,1) | | -0.75 | | 0.36 | | | 0.23 | -0.36 | 0.24 | 184.13 | 0.64 |
| S.E. | | | 0.09 | | 0.15 | | | 0.10 | 0.13 | 0.08 | | |
| $CH_4$ | (0,1,1) | | -0.65 | | | | | 0.28 | -0.43 | 0.21 | 185.88 | 0.65 |
| S.E. | | | 0.09 | | | | | 0.11 | 0.15 | 0.08 | | |
| | | | | | | Monthly | | | | | | |
| $CO_2$ | (0,0,0) | | | | 0.73 | | | 0.24 | | -0.31 | 42.58 | 0.48 |
| S.E. | | | | | 0.10 | | | 0.10 | | 0.10 | | |
| $CO_2$ | (0,0,0) | | | | 0.71 | 0.15 | | 0.27 | | -0.32 | 43.55 | 0.45 |
| S.E. | | | | | 0.10 | 0.10 | | 0.10 | | 0.10 | | |
| $CO_2$ | (0,0,0) | | | | 0.73 | | | 0.27 | 0.15 | -0.26 | 43.88 | 0.46 |
| S.E. | | | | | 0.10 | | | 0.10 | 0.10 | 0.10 | | |
| $CH_4$ | (0,0,1) | | 0.72 | | 0.74 | | | | -0.26 | 0.21 | 38.85 | 0.41 |
| S.E. | | | 0.18 | | 0.14 | | | | 0.12 | 0.07 | | |

**Table S8.** Best-fit results from Autoregressive Integrated Moving Average (ARIMA) showing the top selected model (lowest corrected Akaike Information Criterion, AICc < 2). Models are separated by greenhouse gas (GHG) flux as carbon dioxide fluxes ($CO_2$) and methane fluxes ($CH_4$) as well as by timescale (daily, weekly, monthly). Environmental predictors included: Surface temperature (Surface Temp, °C), dissolved oxygen saturation (DO Sat, %), Chlorophyll-*a* (Chl-a, μg $L^{-1}$), fluorescent dissolved organic matter (fDOM, RFU), inflow discharge (Inflow, $m^3$ $s^{-1}$), and thermocline depth (Thermo. depth, m). Model order is specified as (p,d,q) where p is the order of the AR term, d is the order of the integration term, and q is the order of the MA term. Results for all models with 2 AICc of the best fitting model are included. The root mean square error (RMSE) is also reported for each model. Shaded model results are included in the main manuscript (Table 1). S.E. is the standard error.

| | 25th Percentile | Median | 75th Percentile | p-value |
|---|---|---|---|---|
| | **$CO_2$ (µmol $m^{-2}$ $s^{-1}$)** | | | |
| Intermittent ice-on (Year 1) | 0.12 | 0.71 | 1.34 | <0.001 |
| Continuous Ice-on (Year 2) | -0.34 | 0.28 | 0.93 | |
| | **$CH_4$ (µmol $m^{-2}$ $s^{-1}$)** | | | |
| Intermittent ice-on (Year 1) | -0.001 | 0.001 | 0.004 | <0.001 |
| Continuous Ice-on (Year 2) | -0.002 | -0.001 | 0.000 | |

**Table S9.** 25th percentile, median, and 75th percentile reported measured eddy covariance (EC) data for carbon dioxide ($CO_2$, µmol $m^{-2}$ $s^{-1}$) and methane ($CH_4$, µmol $m^{-2}$ $s^{-1}$) fluxes during winter 2020-2021 (year 1) under partial ice-on ('On') and during winter 2021-2022 (year 2) under continuous ice-on. The Mann-Whitney-Wilcoxon test was used to identify medians which were statistically different. Statistically significant relationships are highlighted in grey.